UNITED NATIONS EDUCATIONAL, SCIENTIFIC AND CULTURAL ORGANIZATION
INTERNATIONAL ATOMIC ENERGY AGENCY
INTERNATIONAL CENTRE FOR THEORETICAL PHYSICS
I.C.T.P., P.O. BOX 586, 34100 TRIESTE, ITALY, CABLE: CENTRATOM TRIESTE

SMR.998c - 14

Research Workshop on Condensed Matter Physics
30 June - 22 August 1997
MINIWORKSHOP ON
PATTERN FORMATION AND SPATIO-TEMPORAL CHAOS
28 JULY - 8 AUGUST 1997

"3D pattern selection and Turing-Hopf interaction" Part II

A. DE WIT
Universite Libre de Bruxelles
Service de Chimie-Physique
Centre for Nonlinear Phenomena & Complex Systems
Blvd. du Triomphe
CP 231, Campus Plaine
1050 Brussels
FRANCE

These are preliminary lecture notes, intended only for distribution to participants.

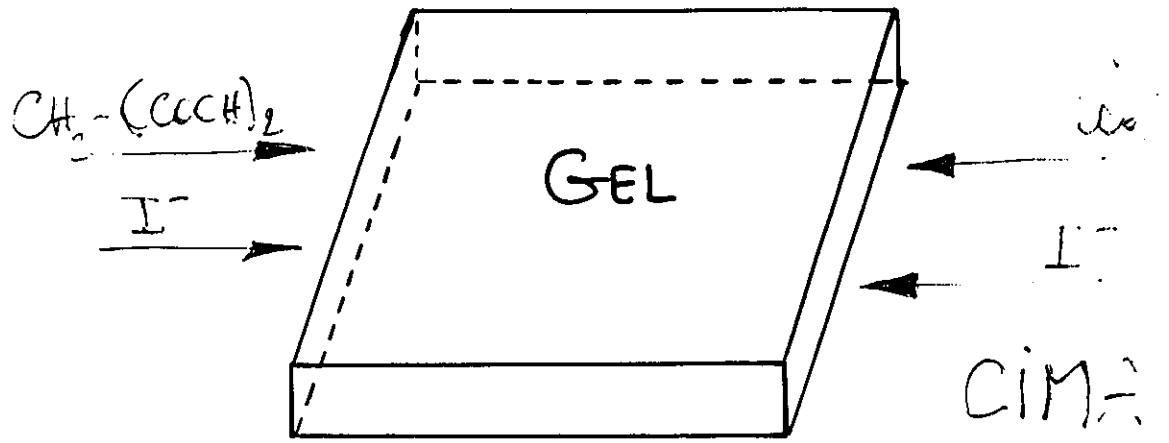

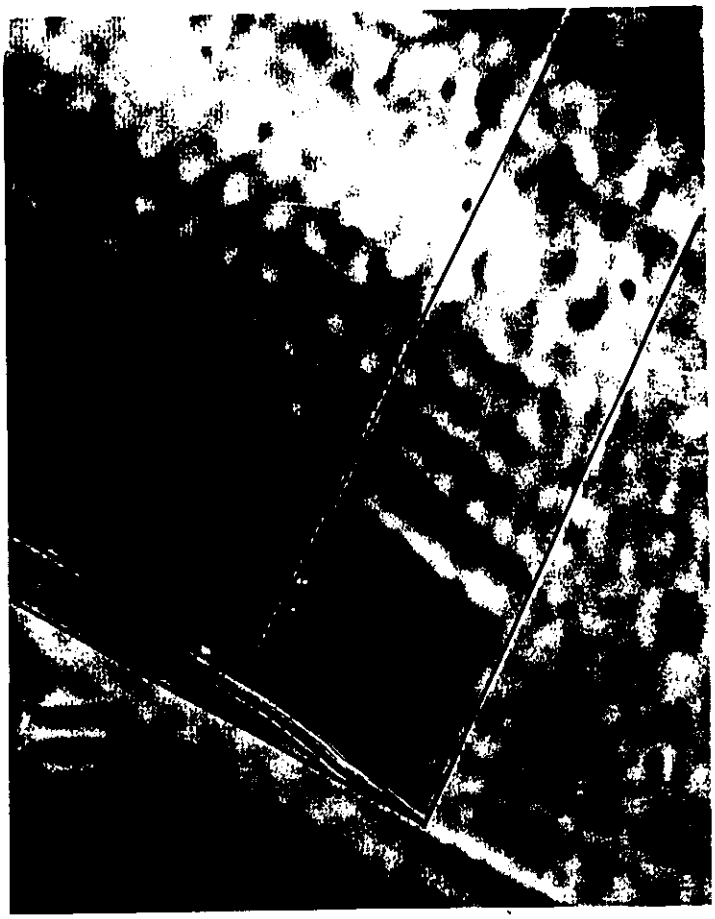

3D spatial structure

J.J. Pesraud et al. Physica A 188, p.1 (1992).

3D

$m = 1$: lamellae

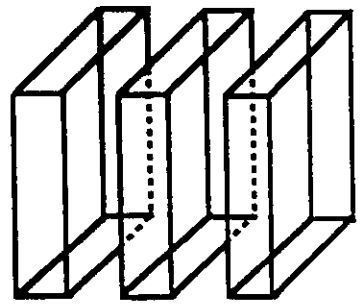

$m = 3$: hexagonal prisms

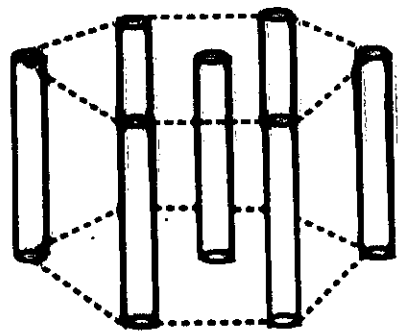

+ new possibilities

$m = 6$: bcc

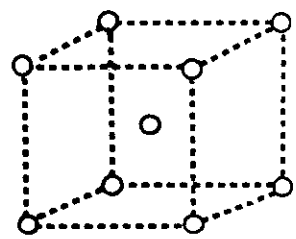

Bifurcation diagram : Walgraef et al.
Adv. Chem. Physics, 49 (198

Simulations : De Wit et al., Physica D, 61 (1992)

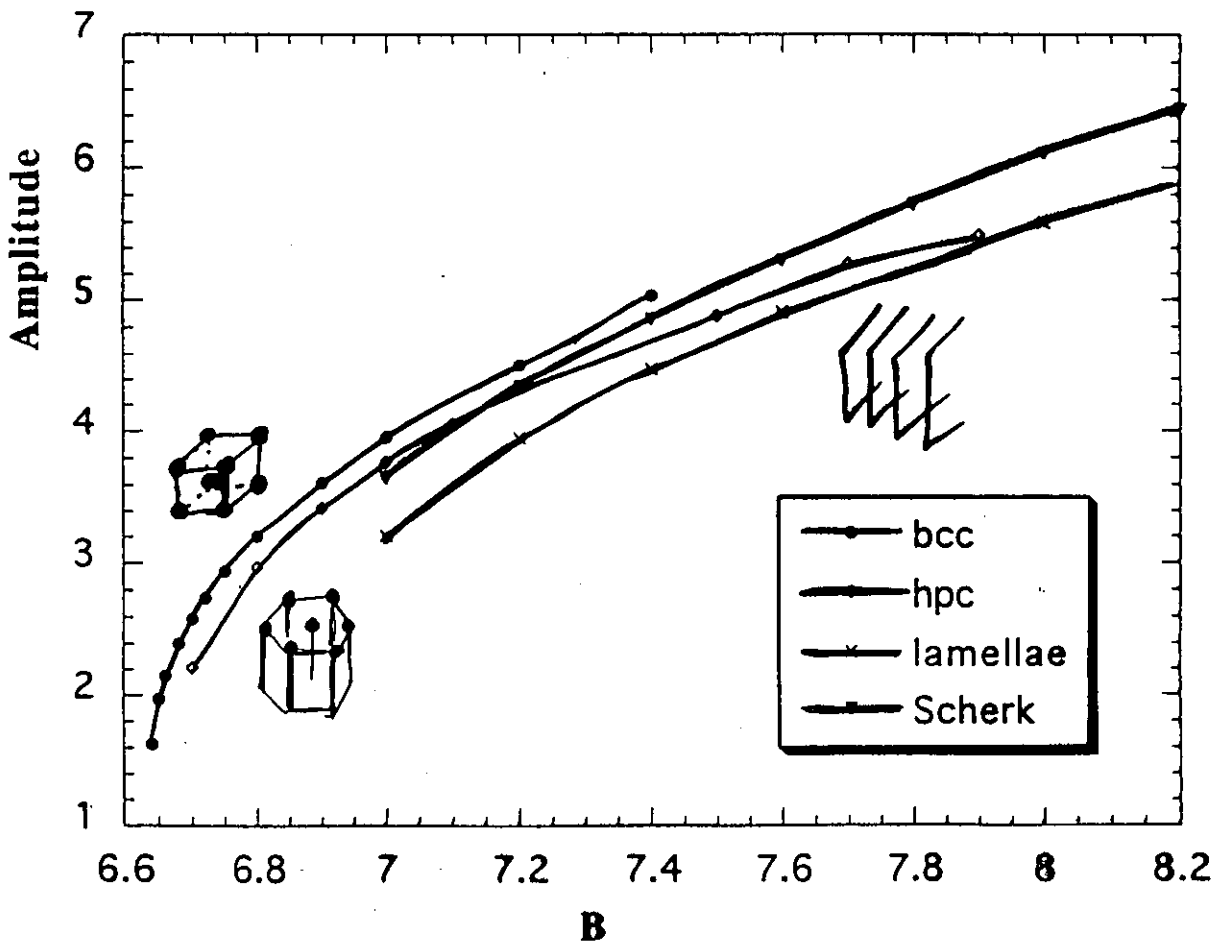

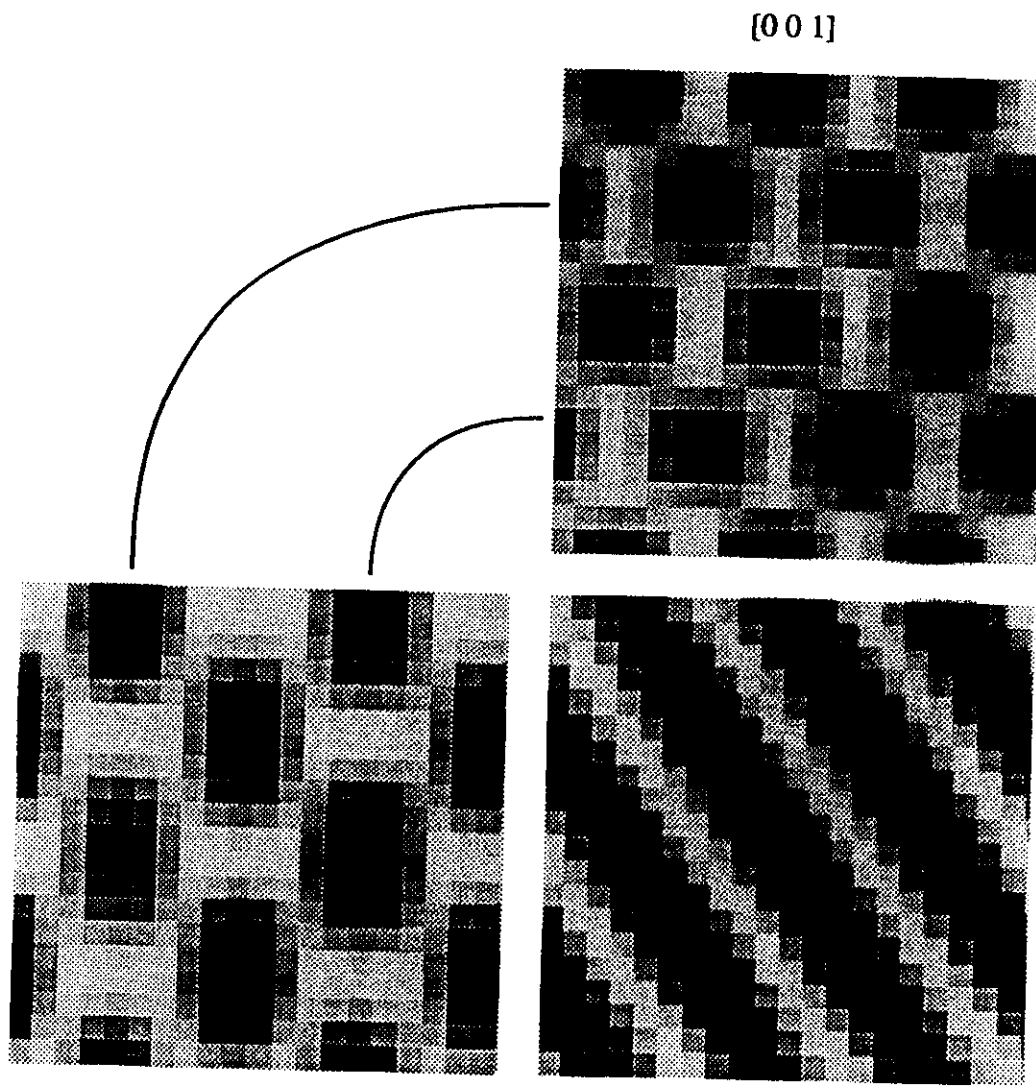
[0 0 1]
[1 0 0]
[0 1 0]

[0 0 1]

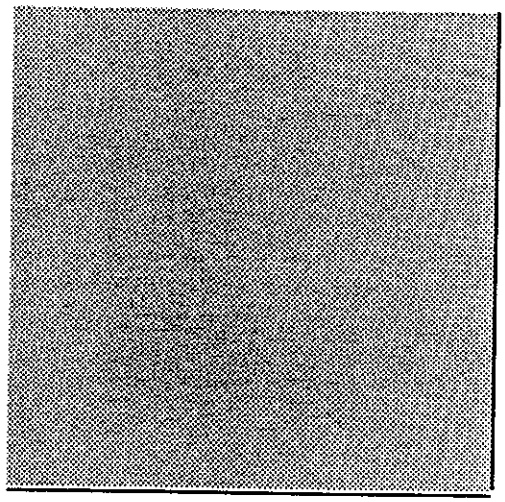

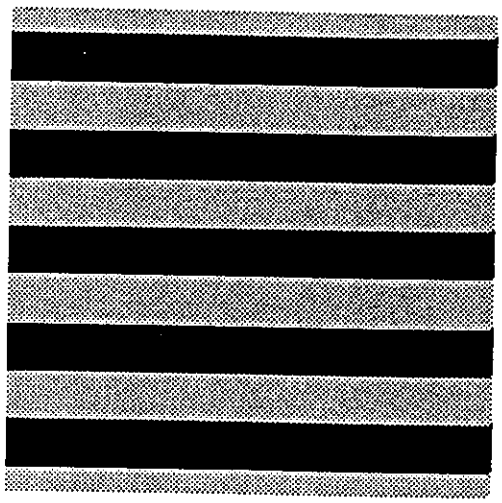

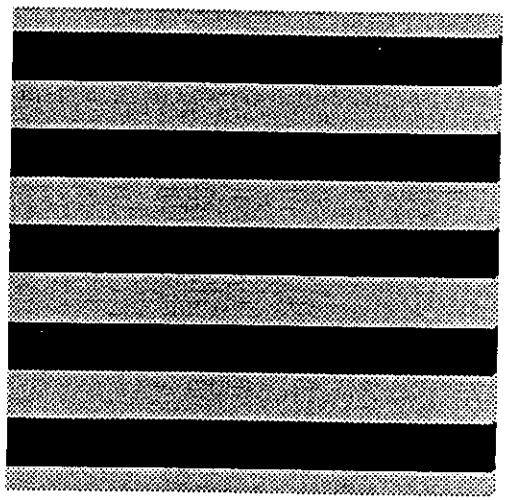

[1 0 0]

[0 1 0]

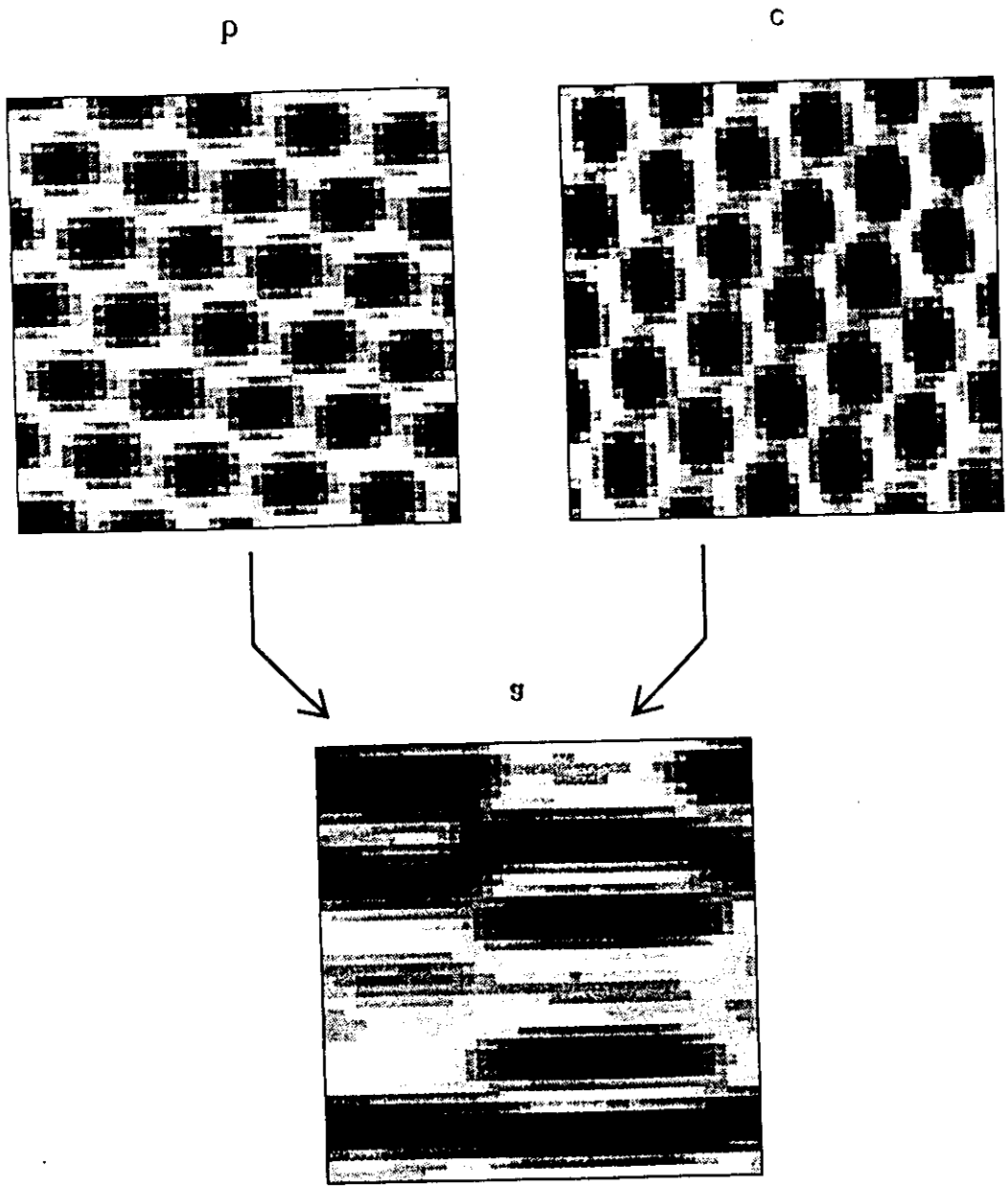
p
c
g

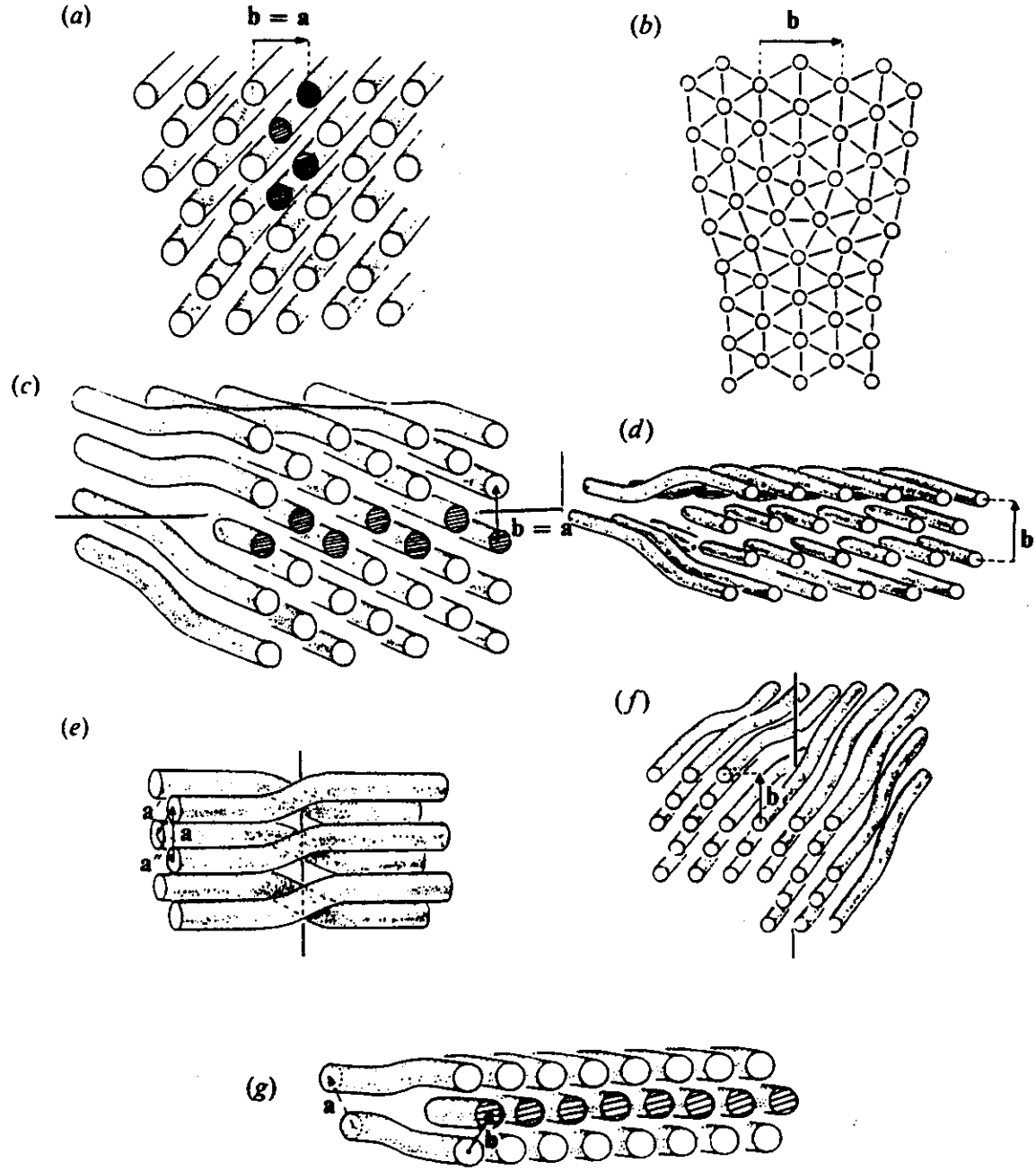

Fig. 6.4.3. Dislocations in the columnar phase: (*a*) and (*b*) longitudinal edge dislocations; (*c*) and (*d*) transverse edge dislocations; (*e*) and (*f*) screw dislocations; (*g*) a hybrid of screw and edge dislocations. It should be noted that the Burgers vector $\mathbf{b} = \mathbf{a}$ for (*a*), (*c*), (*e*) and (*g*), and $\mathbf{b} = \mathbf{a} - \mathbf{a}'$ for (*b*), (*d*) and (*f*). (Bouligand.[61])

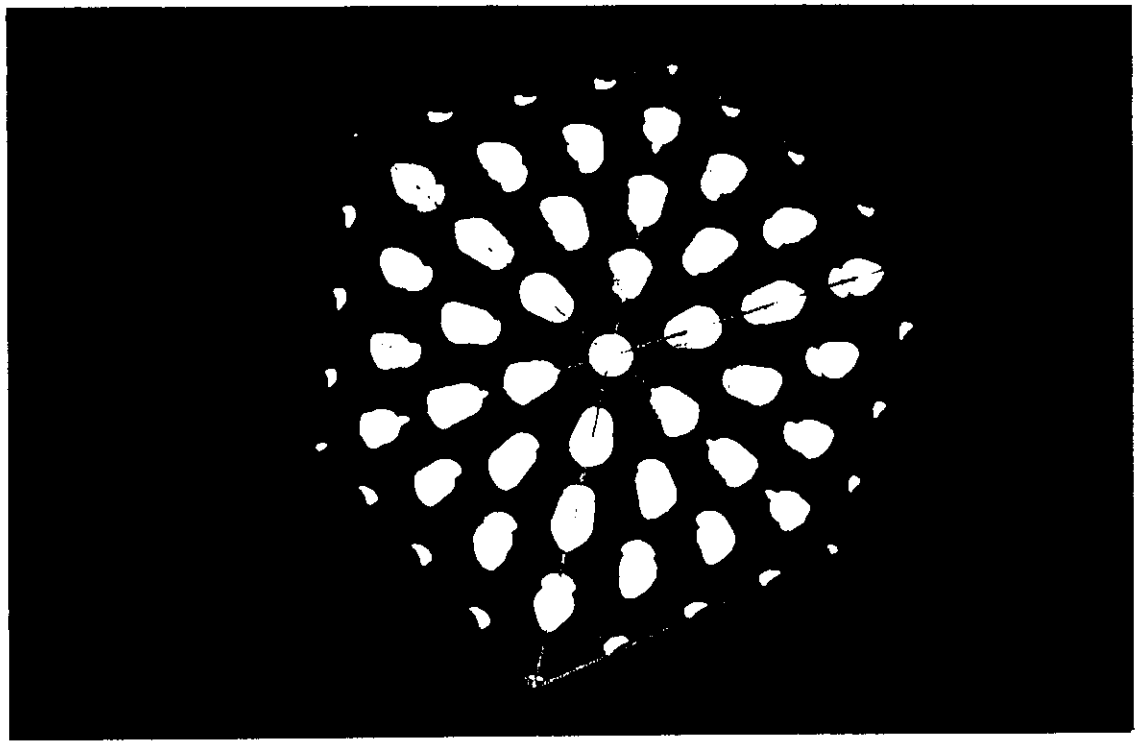

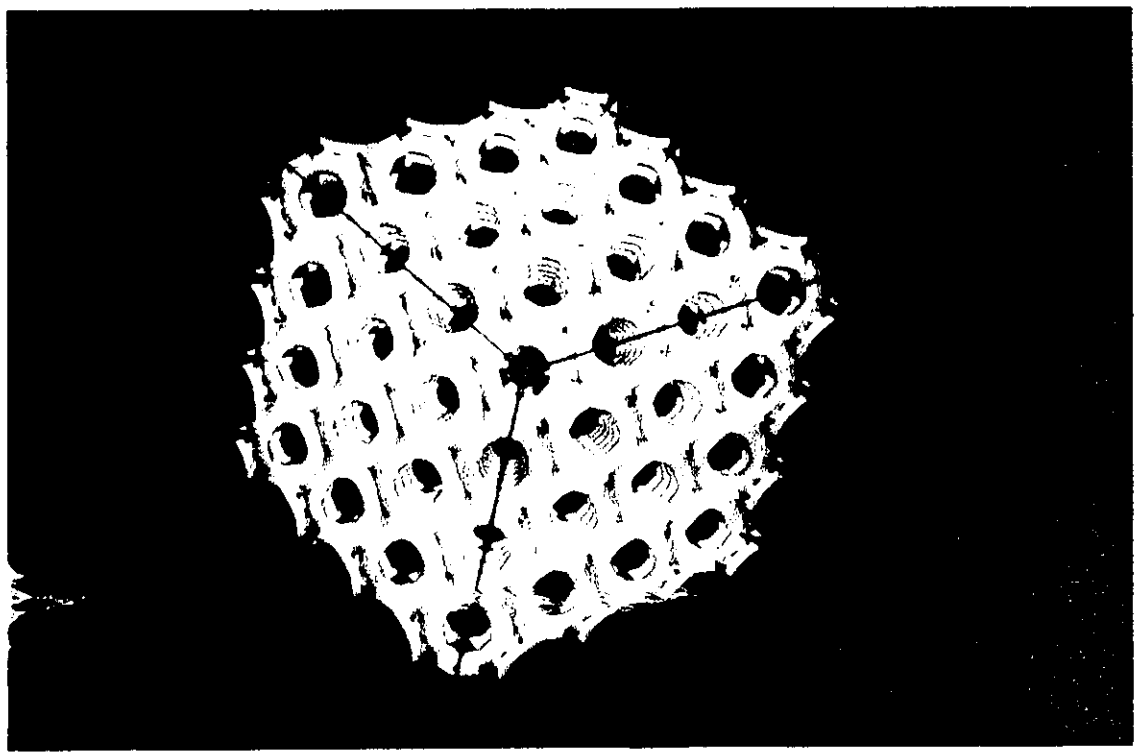

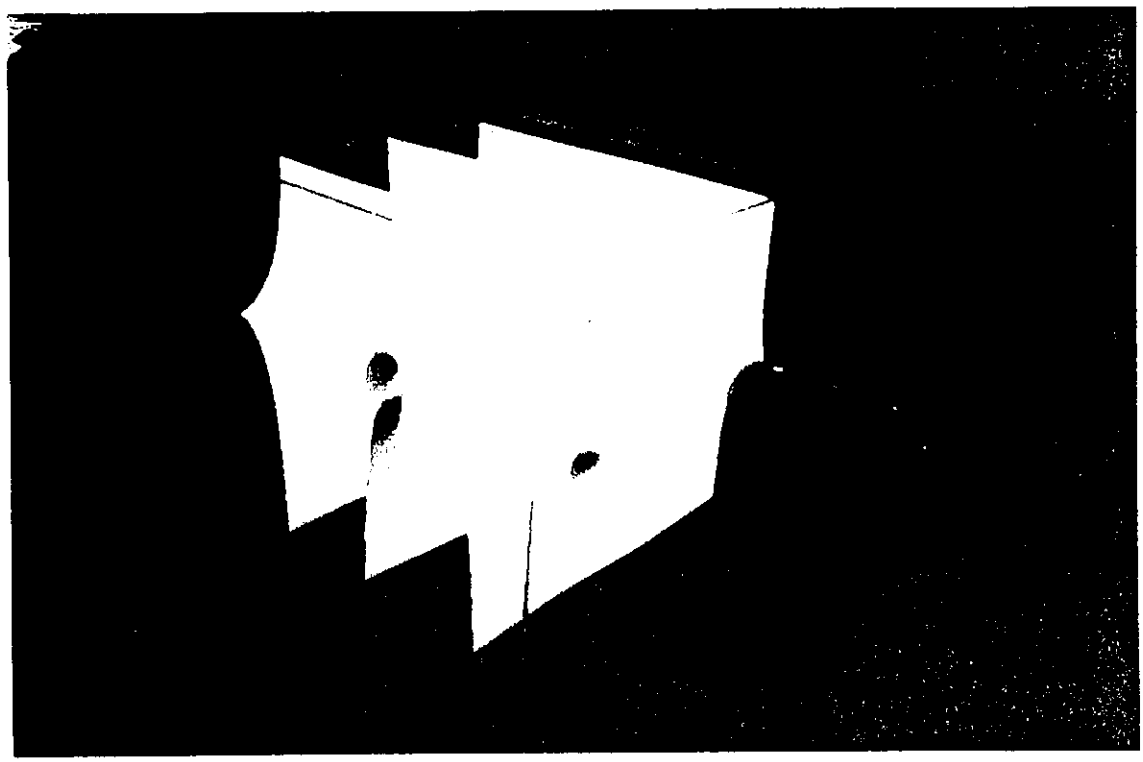

Scherk (Type I)
Minimal Surface

Minimal surfaces

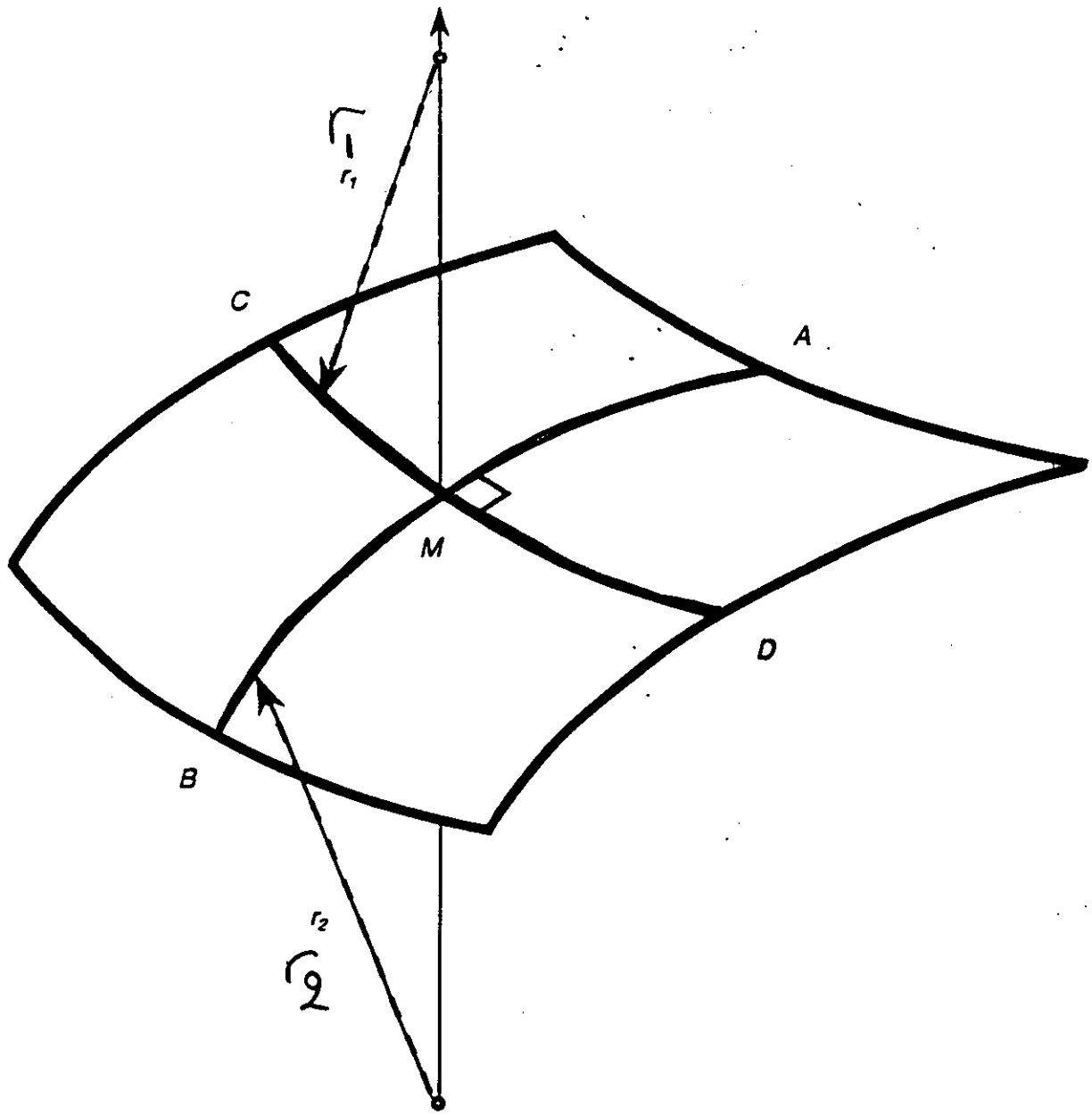

Mean curvature $H = \frac{1}{2}\left(\frac{1}{r_1} + \frac{1}{r_2}\right)$

⟶ $H = 0$ at each point of the surface

Analog structures are obtained experimentally in diblock copolymers

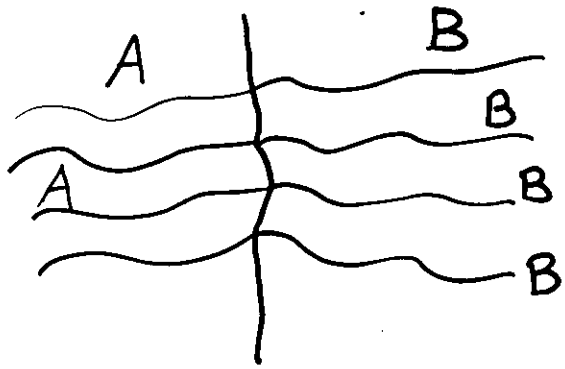

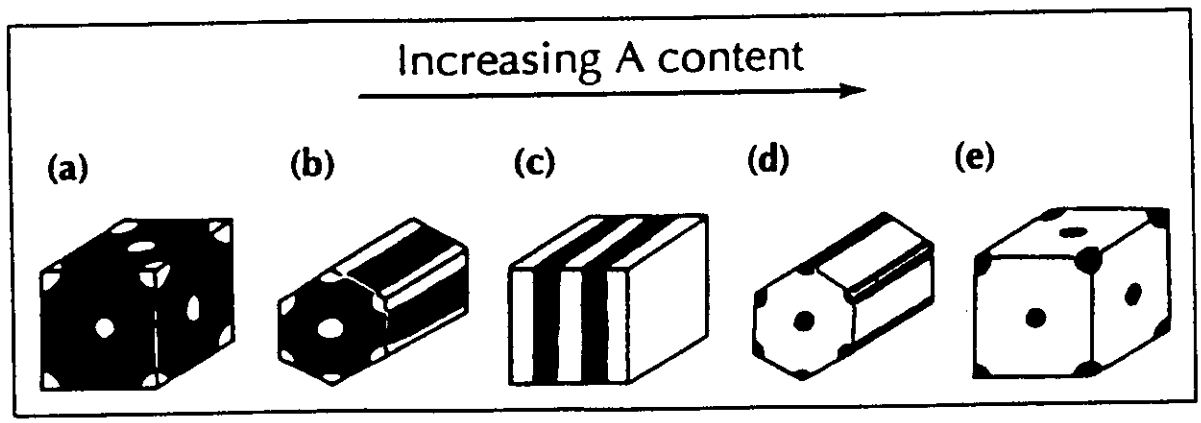

In these systems, Schoen surfaces as well as other minimal surfaces are also seen experimentally

Thomas et al., Nature 334, p. 598 (1988)

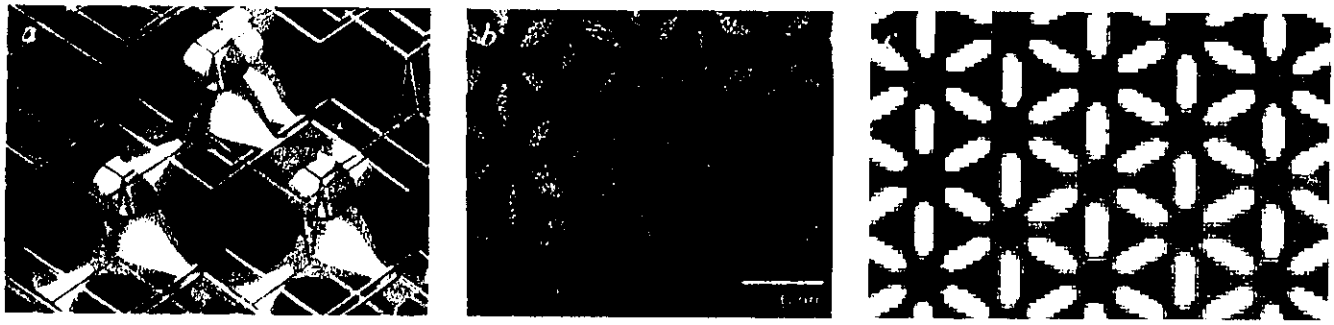
a
b

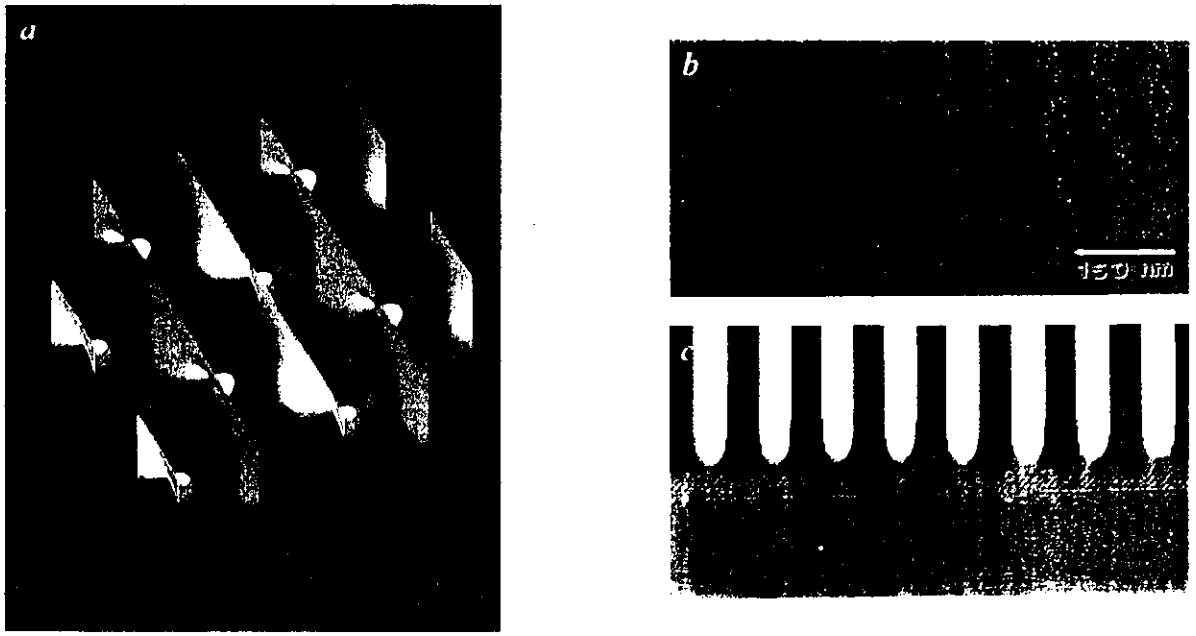
a
b
150 nm
c

One-Dimensional "Spirals": Novel Asynchronous Chemical Wave Sources

J.-J. Perraud,[1] A. De Wit,[2] E. Dulos,[1] P. De Kepper,[1] G. Dewel,[2] and P. Borckmans[2]

[1]*Centre de Recherche Paul Pascal, Université de Bordeaux I, Avenue A. Schweitzer, 33600 Pessac, France*

[2]*Service de Chimie-Physique/Center for Nonlinear Phenomena and Complex Systems, CP231-Université Libre de Bruxelles, 1050 Bruxelles, Belgium*

(Received 30 November 1992)

We report the experimental observation of an endogeneous antisymmetric wave source in a quasi-one-dimensional chemical system. Substantiated by numerical simulations, a theoretical interpretation relying on the interaction between Turing and Hopf modes is proposed.

PACS numbers: 82.20.Mj, 05.70.Ln

The stationary periodic patterns proposed by Turing, in 1952 [1], as a basis for morphogenesis, have only recently been observed [2] in the monophasic isothermal chlorite-iodide-malonic acid (CIMA) reaction [3,4]. The formation of a reversible complex of reduced mobility between activator iodine species and the starch used as a color indicator, creates the difference between the effective diffusivities of the activator and the other unbound species, i.e., chlorite, on which the Turing structures rely for their existence [5]. Indeed, when complexation is progressively relaxed, the experiments show [6,7] that a transition from standing periodic structures to time dependent phenomena in the form of traveling waves may occur. In the transition region, among a wealth of other spatiotemporal behaviors, we report the observation of endogeneous 1D sources emitting waves asynchronously to the left and to the right. We bring proof that these peculiar sources correspond to a localized stationary Turing state embedded in an oscillating background. They are thus of a nature different from that of various sources that have recently been observed in hydrodynamical problems [8,9].

The observation of Turing structures in a nonbiological relatively simple redox reaction was made possible by the use of new continuously fed spatial gel reactors [10] that are a prerequisite for reaching the asymptotic states and for testing their stability at a controlled distance from thermodynamic equilibrium. The original work has sparked off subsequent experimental [6,7,11–13] and theoretical [14,15] studies devoted to the determination of the role played by the gel matrix and the starch, the uncovering of the different possible pattern modes, and the understanding of the role of the feeding concentration ramps.

Our reactor (Fig. 1) consists of a rectangular thin strip of agarose gel, loaded with starch, and fed along two opposite sides from well stirred tanks containing nonreacting subsets of the reagents of the CIMA reaction. Malonic acid is introduced only in tank A and chlorite only in tank B. Reagents diffuse into the gel where reaction processes take place. If no spatial symmetry breaking instability occurs, concentration profiles establish naturally into isoconcentration planes parallel to the feed surfaces. High iodide concentrations are typically found along tank A and a dark blue band due to the formation of a starch-iodine-iodide complex is formed. On the opposite side, iodide and iodine are rapidly oxidized to iodate and the gel remains clear. Beyond critical conditions, Turing structures appear that break this symmetry due to the feeding.

As predicted by the invoked complexation and immobilization mechanism [5], a transition between stationary periodic (Turing modes) and propagating wavelike (Hopf modes) patterns is experimentally observed by decreasing the starch concentration [6]. At very low concentration, only waves could be observed. The starch content is, however, not an easily tunable parameter since its modification requires the manufacturing of a different strip. Nevertheless, a similar transition occurs for a given low enough starch concentration, by increasing the concentration of malonic acid. The possibility of independently tuning two bifurcations by varying two independent parameters is suggestive of the neighborhood of a

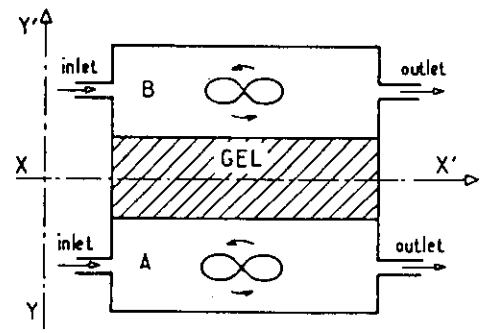

FIG. 1. In the reactor the gel strip is 10 mm long (XX' direction), 3 mm wide (YY' direction), and 0.14 mm thick. It is prepared by rapidly cooling a hot solution containing 0.9 g of Thiodène (a soluble starch from Prolabo) and 1 g of Agarose (Fluka 05070) in 50 ml of deionized water. It is then compressed between a white bottom plate and a transparent glass cover. Two opposite sides are in contact with the feeding tanks and the others with impermeable boundaries. $T=(2\pm0.5)$ °C. The feed concentrations are (i) tank A $[KI]=2.5\times10^{-3}M$, $[CH_3CO_2H]=2.3M$, $[CH_2(CO_2H)_2]$ is the tunable parameter; (ii) tank B $[KI]=2.5\times10^{-3}M$, $[NaClO_2]=2.4\times10^{-2}M$, $[NaOH]=2.0\times10^{-2}M$.

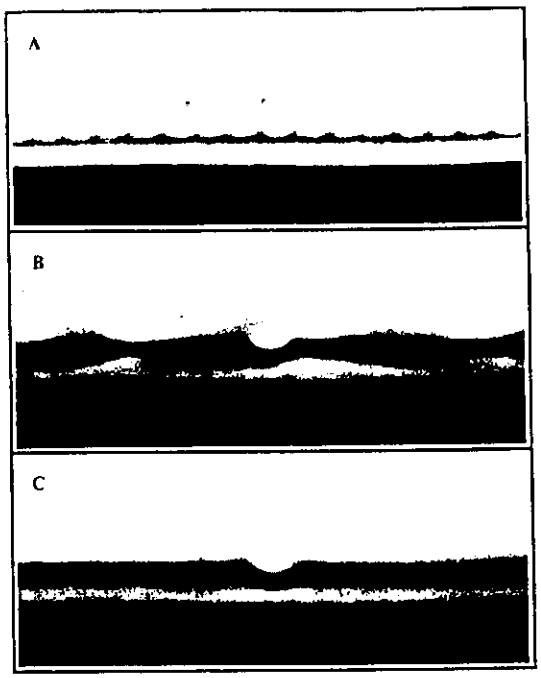

FIG. 2. (a) String of stationary Turing spots: Line of standing clear spots of oxidized state embedded in a band of the reduced darker state organized parallel to the feed boundaries (see Fig. 1); $[CH_2(CO_2H)_2]=0.5\times10^{-2}M$. (b) Antisymmetric pacemaker in a wave train state: Waves travel parallel to the feed boundaries with arrowhead shape. The clear edge of oxidation propagates into the darker recovery region with a rate of about 3 mm/min. The clear isolated Turing-like spot, near the middle of the figure, acts as an antisynchronous wave source. $[CH_2(CO_2H)_2]=1.0\times10^{-2}M$. (c) State averaged pattern obtained by averaging the dynamics of the wave train pattern (b) over several periods.

codimension 2 point.

Thus for a range of feed concentrations low in malonic acid, a Turing structure restricted to a narrow region can be obtained [Fig. 2(a)]: It forms a single line of clear spots, parallel to the feed boundaries, with a wavelength $\lambda=0.17\pm0.01$ mm. On comparing λ with the thickness of the gel strip (0.14 mm), one can infer that the pattern is effectively one dimensional. If the malonic acid concentration is then doubled, the bright spots die out while oscillatory behavior develops. After some time only wave trains remain, similar to those observed by Agladze, Dulos, and DeKepper [6], traveling parallel to the feed boundaries.

Very often, however, even after several hours, a few single bright spots (one to three) do not disappear and act as genuine 1D antisynchronous sources of wave trains [Fig. 2(b)]. The phenomenon is best represented by a space-time plot of the dynamics along a line parallel to the feed direction, passing through the source [Fig. 3(a)]. Clear bands of maximum intensity spread, alternatively to the right and to the left, with a time delay of 16 s, from a small region that essentially remains time invariant. The existence of a permanently brighter state at the wave source is clearly demonstrated in the time average picture [Fig. 2(c)]. Note that the size and relative intensity of the wave source region is similar to that of the individual spots making up the Turing pattern [Fig. 2(a)]. The source thus corresponds to a localized elementary Turing cell. Furthermore, the antiphase property of such a wave source does not result from a continuous spiraling wave in any plane since a time invariant region similar to that of Fig. 3(a) is found in the XX' direction at any vertical position in the YY' direction. The essence of the phenomenon is thus one dimensional [7].

Moreover, on further increasing malonic acid by 30%, all such sources disappear and waves propagate along the whole line. However, on resetting the control parameter to the lower value, isolated sources reappear after a few hours but generally at locations uncorrelated to the previous ones. They are thus truly endogeneous and not linked to defects or impurities trapped in the gel.

From the theoretical point of view, the existence in other fields of localized structures under uniform conditions has been shown in recent studies [16–19] to rely on two ingredients: multistability between various global states and dynamics not deriving from a potential function indicating the influence of so-called nonvariational effects [20,21]. These two elements are present in the vicinity of a Turing-Hopf codimension 2 bifurcation point where a pair of complex conjugate roots and a real root (with a wave number of the linear dispersion relation $|\underline{q}|=q_c\neq0$) simultaneously cross the imaginary axis on varying the bifurcation parameter.

If C is the vector of concentrations, f represents the reaction kinetics, and $\underline{D}$ is the diagonal matrix of positive diffusion coefficients, then near the Turing-Hopf point, the dynamics of a one-dimensional reaction-diffusion system

$$\frac{\partial \mathbf{C}}{\partial t}=\mathbf{f}(\mathbf{C})+\underline{D}\frac{\partial^2\mathbf{C}}{\partial x^2}$$

may be described by the superposition of Turing $T(X,\tau)$ and Hopf $H(X,\tau)$ fields:

$$\mathbf{C}(x,t)=\mathbf{C}_0+\mathbf{e}_T T(X,\tau)e^{iq_c x}+\mathbf{e}_H H(X,\tau)e^{i\Omega_c t}+\text{c.c.}$$

Here, $\mathbf{C}_0$ is the uniform reference state and $\mathbf{e}_T$ and $\mathbf{e}_H$ are respectively the critical Turing and Hopf eigenvectors of the linearized evolution operator. Ω_c is the linear frequency of the Hopf mode, i.e., the imaginary part of the complex root at the codimension 2 point.

The competition between such modes is then described by amplitude equations [22,23]. If X and τ are the slow space and time scales then

$$\frac{\partial T}{\partial \tau}=\mu_T T-g|T|^2T-\lambda|H|^2T+D^T\frac{\partial^2 T}{\partial X^2},$$

$$\frac{\partial H}{\partial \tau}=\mu_H H-(\beta_r+i\beta_i)|H|^2H-(\delta_r+i\delta_i)|T|^2H+(D_r^H+iD_i^H)\frac{\partial^2 H}{\partial X^2},$$

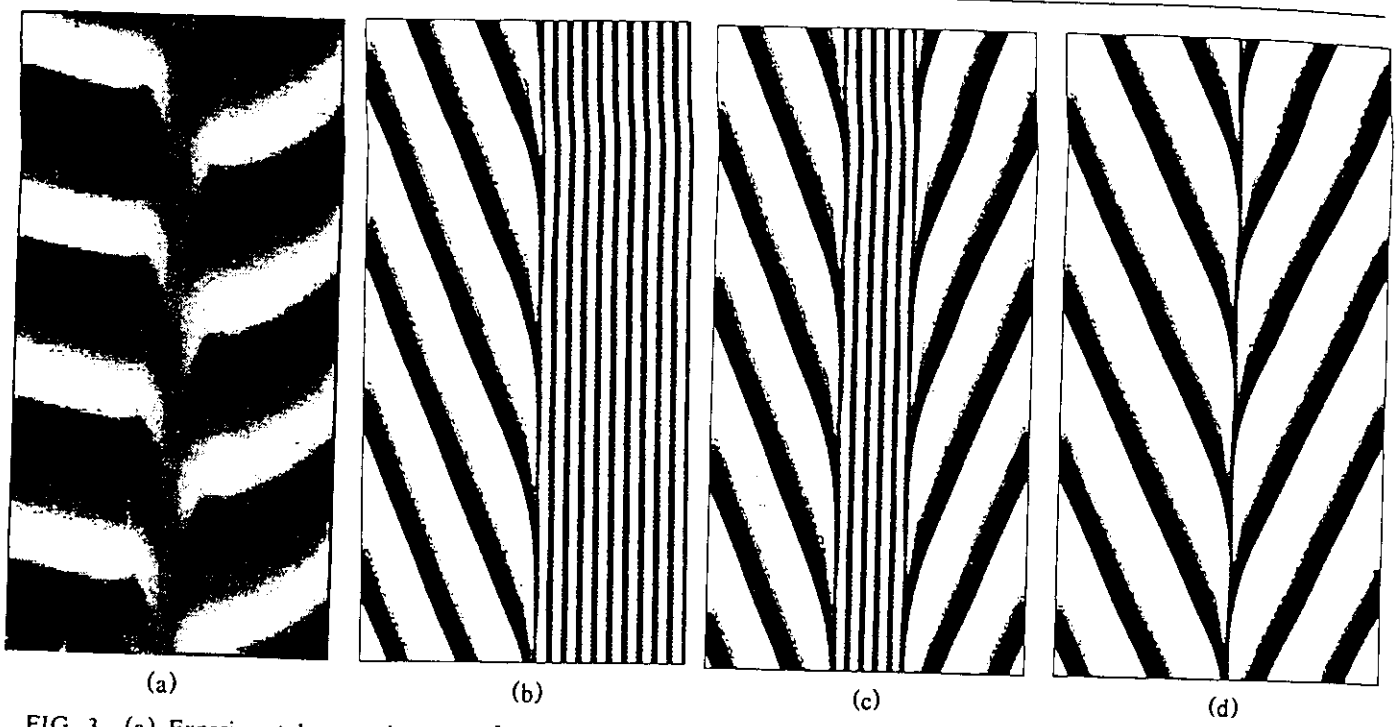

FIG. 3. (a) Experimental space-time map [space: horizontal axis; time: vertical axis (running upwards)]. The light intensity along a line parallel to the feed boundaries, passing through the brightest part of the pacemaker, is plotted as a function of time. Bright lines correspond to clear wave fronts. The field view corresponds to 1.6 mm. The numerical space-time maps (b)–(d) are produced by integrating the reaction-diffusion equations of the 1D Brusselator model with an implicit integration scheme complemented with a finite difference method ($L=250$, $t=20$ adimensional units). No flux boundaries are assumed. The following values of the parameters are used: $A=2.5$, $D_X=4.11$, $D_Y=9.73$. Then both global Turing and Hopf modes are separately stable [24]. B is used as bifurcation parameter in this near codimension 2 situation. (b) Pinned front connecting a Turing pattern (right) to a train of plane waves (left) for $B=10.0$. (c) Droplet of a Turing structure embedded in a Hopf background emitting plane waves on both sides ($B=10.0$). (d) Endogeneous 1D spiral obtained by increasing in one step B to 12.5 starting from the front in (b). The waves are always emitted in phase opposition to the left and to the right. Multistability between such spirals, fronts, and localized Turing states is obtained for the same range of parameters. As an example, the localized structures (b) and (c) are still stable at $B=12.5$ if B is increased quasistatically in small steps.

where μ_T and μ_H are the two unfolding parameters. We assume in the following that D^T and D_r^H are positive and also g, β_r so that both bifurcations are supercritical. The above equations have in general a nonvariational structure. This dynamical system possesses three nontrivial global solutions: (i) a family of Turing structures

$$T=[(\mu_T-D^TQ^2)/g]^{1/2}e^{iQX},\quad H=0;$$

(ii) a one-parameter family of plane waves

$$T=0,\quad H=[(\mu_H-D_r^H\kappa^2)/\beta_r]^{1/2}e^{i(\Omega_\kappa\tau-\kappa X)}$$

with the frequency renormalization: $\Omega_\kappa=-\beta_i|H_\kappa|^2-D_i^H\kappa^2$, where H_κ is the preexponential factor in H; and (iii) a two-parameter family of mixed modes that we do not write down explicitly as we concentrate, among the many possible scenarios, on situations where the mixed modes are unstable and the system exhibits bistability between the pure global Turing and Hopf modes.

The ingredients to stabilize localized structures are therefore present. These may be formed by spatial juxtaposition of the global states as is corroborated by numerical simulations on the Brusselator [24], in the vicinity of such a codimension 2 point.

The simplest localized structure consists of a front [Fig. 3(b)] connecting a Turing pattern domain to a train of plane waves the wave vector and frequency of which are selected by the nonlinear dispersion relation. Since the width of the front is narrow, it may interfere with the underlying Turing structure leading to its pinning. As a result a stationary front is obtained for a finite range (locking band) of the bifurcation parameter values [25,26]. Beyond, but near the depinning transition, one observes, on the simulations, the characteristic oscillating velocity of the front. One wavelength to the Turing structure is added (subtracted) during every emitted wave period. The nonadiabatic effects responsible for this pinning escape standard amplitude equations analysis.

Those fronts may then serve as "building blocks" to construct droplets of one global state embedded into another [20,21,27–29]. Simulations have indeed produced such localized one-dimensional objects the core of which is formed by a Turing structure, truncated to a few wavelengths, emitting plane waves to both sides [Fig. 3(c)]. The amplitude of the plane waves goes to zero in

the core where conversely the Turing mode presents a local maximum but is absent elsewhere. We claim that the stability of such symbiotic Hopf hole and Turing pulse finds its origin in a combination of the pinning and nonvariational effects.

The number of wavelengths in the core and the phase relation between the waves emitted to the left and the right depend strongly on the initial conditions as intricate hysteresis effects are present. On varying the bifurcation parameter in the direction where the global Hopf mode becomes dominant, antisynchronous wave sources, analogous to the experimental ones, can readily be obtained [Fig. 3(d)]. They can be thought of as 1D spirals.

Simulations also produce the complementary localized structures where the Hopf mode is embedded in the Turing background. Such objects and localized Turing structures restricted to three wavelengths in the core have been observed transiently in experiments, suggesting a narrower range of stability or smaller basin of attraction.

These latter experimental observations, for parameters in the range for which the wave sources occur, comfort us in the belief that the competition between the Turing and Hopf modes is indeed important to explain the origin of all these localized sources.

We thank J. Boissonade, A. Arneodo, and D. Walgraef for stimulating discussions. P.B. and G.D. are Research Associates with the FNRS (Belgium) and A.D. is an IRSIA (Belgium) Fellow. This work was supported by the EC Science Program (Twinning No. SC1-CT91-0706). Centre de Recherche Paul Pascal is CNRS UP 78476.

[1] A. M. Turing, Philos. Trans. R. Soc. London, Ser. B **327**, 37 (1952).
[2] V. Castets, E. Dulos, J. Boissonade, and P. De Kepper, Phys. Rev. Lett. **64**, 2953 (1990).
[3] P. De Kepper, I. R. Epstein, K. Kustin, and M. Orban, J. Phys. Chem. **86**, 170 (1982).
[4] I. Lengyel, G. Rabai, and I. R. Epstein, J. Am. Chem. Soc. **112**, 4606 (1990); **112**, 9104 (1990).
[5] I. Lengyel and I. R. Epstein, Proc. Natl. Acad. Sci. USA **89**, 3977 (1992).
[6] K. Agladze, E. Dulos, and P. De Kepper, J. Phys. Chem. **96**, 2400 (1992).
[7] J.-J. Perraud, K. Agladze, E. Dulos, and P. De Kepper, Physica (Amsterdam) **188A**, 1 (1992).
[8] D. Bensimon, P. Kolodner, C. M Surko, H. Williams, and V. Croquette, J. Fluid Mech. **217**, 441 (1990).
[9] *Order and Turbulent Patterns in Taylor-Couette Flow*, edited by D. C. Andereck and F. Hayot (Plenum, New York, 1992).
[10] Z. Noszticzius, W. Horsthemke, W. D. McCormick, H. L. Swinney, and W. Y. Tam, Nature (London) **329**, 619 (1987).
[11] P. De Kepper, V. Castets, E. Dulos, and J. Boissonade, Physica (Amsterdam) **49D**, 161 (1991).
[12] Q. Ouyang and H. L. Swinney, Nature (London) **352**, 610 (1991).
[13] Q. Ouyang and H. L. Swinney, Chaos **1**, 411 (1991).
[14] P. Borckmans, A. De Wit, and G. Dewel, Physica (Amsterdam) **188A**, 137 (1992).
[15] V. Dufiet and J. Boissonade, J. Chem. Phys. **96**, 664 (1992).
[16] G. Ahlers, Physica (Amsterdam) **51D**, 421 (1991), and references therein.
[17] U. Middya, M. Sheintuch, M. D. Graham, and D. Luss, Physica (Amsterdam) **63D**, 393 (1993).
[18] H. Willebrand, T. Hünteler, F.-J. Niedernostheide, R. Dohmen, and H.-G. Pruwins, Phys. Rev. A **45**, 8766 (1992).
[19] H. H. Rotermund, S. Jakubith, A. von Oertzen, and G. Ertl, Phys. Rev. Lett. **66**, 3083 (1991).
[20] O. Thual and S. Fauve, J. Phys. (Paris) **49**, 182 (1988).
[21] W. van Saarloos and P. C. Hohenberg, Physica (Amsterdam) **D56**, 303 (1992).
[22] J. Guckenheimer and P. Holmes, *Nonlinear Oscillations, Dynamical Systems and Bifurcations of Vector Fields* (Springer, New York, 1983).
[23] H. Kidachi, Prog. Theor. Phys. **63**, 1152 (1980).
[24] G. Nicolis and I. Prigogine, *Self-Organization in Nonequilibrium Systems* (Wiley, New York, 1977).
[25] Y. Pomeau, Physica (Amsterdam) **23D**, 3 (1986).
[26] D. Bensimon, B. I. Shraiman, and V. Croquette, Phys. Rev. A **38**, 5461 (1988).
[27] S. Koga and Y. Kuramoto, Prog. Theor. Phys. **63**, 106 (1980).
[28] V. Hakim, P. Jakobsen, and Y. Pomeau, Europhys. Lett. **11**, 19 (1990).
[29] G. Dewel and P. Borckmans, Europhys. Lett. **17**, 523 (1992).

Chaotic Turing-Hopf mixed mode

Last copy. Please, don't remark

A. De Wit, G. Dewel, and P. Borckmans
Service de Chimie Physique and Centre for Nonlinear Phenomena and Complex Systems, Université Libre de Bruxelles, Case Postale 231, 1050 Brussels, Belgium
(Received 6 July 1993)

An alternative scenario for the onset of spatiotemporal chaos in one-dimensional extended systems arising from a phase instability of a Turing-Hopf mixed mode is presented. This mechanism leads to weak and defect turbulences. The transition between these two is either continuous or hysteretic, depending on the values of the parameters.

PACS number(s): 47.20.−k, 05.45.+b

The study of spatiotemporal chaos in driven extended systems has been the focus of a large activity these last years [1]. One scenario has been clearly identified where the Benjamin-Feir instability of a homogeneous limit cycle first drives the system into a regime of weak turbulence [2] followed by a more chaotic state characterized by the proliferation of topological defects (*defect turbulence*) [3,4]. On the other hand, the homogeneous steady states of reaction-diffusion systems may also be destabilized by another type of diffusion-driven instability leading to Turing patterns [5]. These steady periodic concentration structures have now been obtained experimentally in open gel reactors [6,7]. In the region where Turing and Hopf bifurcations interact, spatiotemporal complexity may appear in these experimental patterns [8,9]. The scenario presented above can, however, not explain this "chemical turbulence," as the Benjamin-Feir and the Turing instabilities are mutually exclusive for most reaction-diffusion systems [2,10]. In this Rapid Communication we report an alternative mechanism based on the phase instability of mixed Turing-Hopf modes which may arise in the vicinity of the Turing-Hopf codimension-2 point [11,12]. We focus here on one dimensional (1D) systems.

In the vicinity of this codimension-2 point the concentration field $\mathbf{c}$, which appears in the chosen reaction-diffusion system, may be expressed in terms of two complex amplitudes T and H:

$$\mathbf{c}(x,t) = \mathbf{c}_0 + \mathbf{e}_T T e^{iq_c x} + \mathbf{e}_H H e^{i\omega_c t} + \text{c.c.} \qquad (1)$$

$\mathbf{c}_0$ is the uniform reference state, $\mathbf{e}_T$ and $\mathbf{e}_H$ are respectively the critical Turing and Hopf eigenvectors of the linearized reaction-diffusion operator. ω_c is the critical frequency of the limit cycle while q_c is the critical Turing wave vector. c.c. stands for complex conjugate. The competition between these modes can be described by amplitude equations that are obtained by the use of standard techniques of bifurcation analysis [13]. If X and τ are the slow space and time scales, then [11]

$$\frac{\partial T}{\partial \tau} = \mu_T T - g|T|^2 T - \lambda |H|^2 T + D^T \frac{\partial^2 T}{\partial X^2}, \qquad (2)$$

$$\frac{\partial H}{\partial \tau} = \mu_H H - (\beta_r + i\beta_i)|H|^2 H - (\delta_r + i\delta_i)|T|^2 H + (D_r^H + iD_i^H)\frac{\partial^2 H}{\partial X^2}, \qquad (3)$$

where μ_H and $\mu_T = \mu_H + \nu$ are the two unfolding parameters. We assume in the following that g, β_r, D^T, and D_r^H are positive so that both bifurcations are supercritical.

The dynamical system of Eqs. (2) and (3) possesses three nontrivial global solutions:

(i) a family of Turing structures,

$$T = \left\{ \frac{\mu_T - D^T Q^2}{g} \right\}^{1/2} e^{iQX}, \quad H = 0; \qquad (4)$$

(ii) a one-parameter family of plane waves,

$$T = 0, \quad H = \left\{ \frac{\mu_H - D_r^H K^2}{\beta_r} \right\}^{1/2} e^{i(\Omega_K \tau - KX)} \qquad (5)$$

with the frequency renormalization, $\Omega_K = -\beta_i |H_K|^2 - D_i^H K^2$, where H_K is the preexponential factor in H;

(iii) a two-parameter family of mixed modes,

$$T = \left\{ \frac{\beta_r(\mu_T - D^T Q^2) - \lambda(\mu_H - D_r^H K^2)}{\Delta} \right\}^{1/2} e^{iQX},$$

$$H = \left\{ \frac{g(\mu_H - D_r^H K^2) - \delta_r(\mu_T - D^T Q^2)}{\Delta} \right\}^{1/2} \times e^{i(\Omega_{KQ}\tau - KX)} \qquad (6)$$

with $\Delta = \beta_r g - \lambda \delta_r$ and $\Omega_{KQ} = -\beta_i |H_{KQ}|^2 - \delta_i |T_{KQ}|^2 - D_i^H K^2$, where H_{KQ} and T_{KQ} are the preexponential factors of H and T. The relative stability of these three sets of modes may lead to various bifurcation scenarios. When $\Delta < 0$, the mixed mode is always unstable and bistability between the limit cycle and the Turing mode occurs. Various localized structures have been characterized in this domain [14]. In the following, we concentrate on situations where the mixed modes are stable toward spatially homogeneous perturbations ($\Delta > 0$). This condition can indeed be fulfilled for some range of

1063-651X/93/48(6)/4191(4)/$06.00

parameters in reaction-diffusion systems. On increasing the bifurcation parameter μ_H one then typically observes the following sequence of states (when $\nu > 0$): Turing structures $\rightarrow$ mixed mode $\rightarrow$ homogeneous oscillations. In the absence of spatial modulations, Eqs. (2) and (3) are invariant under the transformations $T \rightarrow Te^{i\theta}$ and $H \rightarrow He^{i\phi}$. As a result, the corresponding linearized matrix about the mixed state has two zero eigenvalues. When spatially inhomogeneous perturbations are taken into account these marginal modes may induce diffusive instabilities of the phases. In particular, the most stable mixed mode ($Q = 0, K = 0$) undergoes such an instability when

$$\mathcal{D} = \frac{D_i^H(\beta_i g - \lambda\delta_i) + D_r^H(\beta_r g - \lambda\delta_r)}{\Delta} < 0. \qquad (7)$$

Let us remark that the standard Benjamin-Feir instability criterion of a homogeneous limit cycle is recovered when all the parameters related to the coupling between the two modes are set equal to zero, i.e.,

$$D_i^H\beta_i + D_r^H\beta_r < 0. \qquad (8)$$

It is important to note that the inequality (7) may be satisfied even when (8) is not fulfilled, i.e., when the limit cycle is stable with respect to the modulational instability.

We have numerically integrated Eqs. (2) and (3) by means of a fourth-order Runge-Kutta scheme (NAG library) complemented by finite-difference methods. The behavior of the system is followed on a system of length $L = 512$ with periodic boundary conditions. These simulations show that, when $\mathcal{D} < 0$, the mixed mode is indeed unstable. According to the value of the parameters, the system enters then either a phase-turbulent regime similar to that of the Kuramoto-Sivashinsky equation [15,16] or a defect chaos regime [2,17] characterized by phase defects and large-amplitude fluctuations on both T and H.

These dynamics can be illustrated by space-time maps of the concentration $\mathbf{c}(x,t)$ and of the amplitude and phase of the Hopf mode (Fig. 1). In the example shown here, the parameters are chosen such that an initially stable mixed mode is brought into a defect chaos regime after one-third of the time run. In the first part of the time, we see that the lines of constant phases are continuous [Fig. 1(a)]. The amplitudes of the Turing and Hopf modes are constant [Fig. 1(b)]. The concentra-

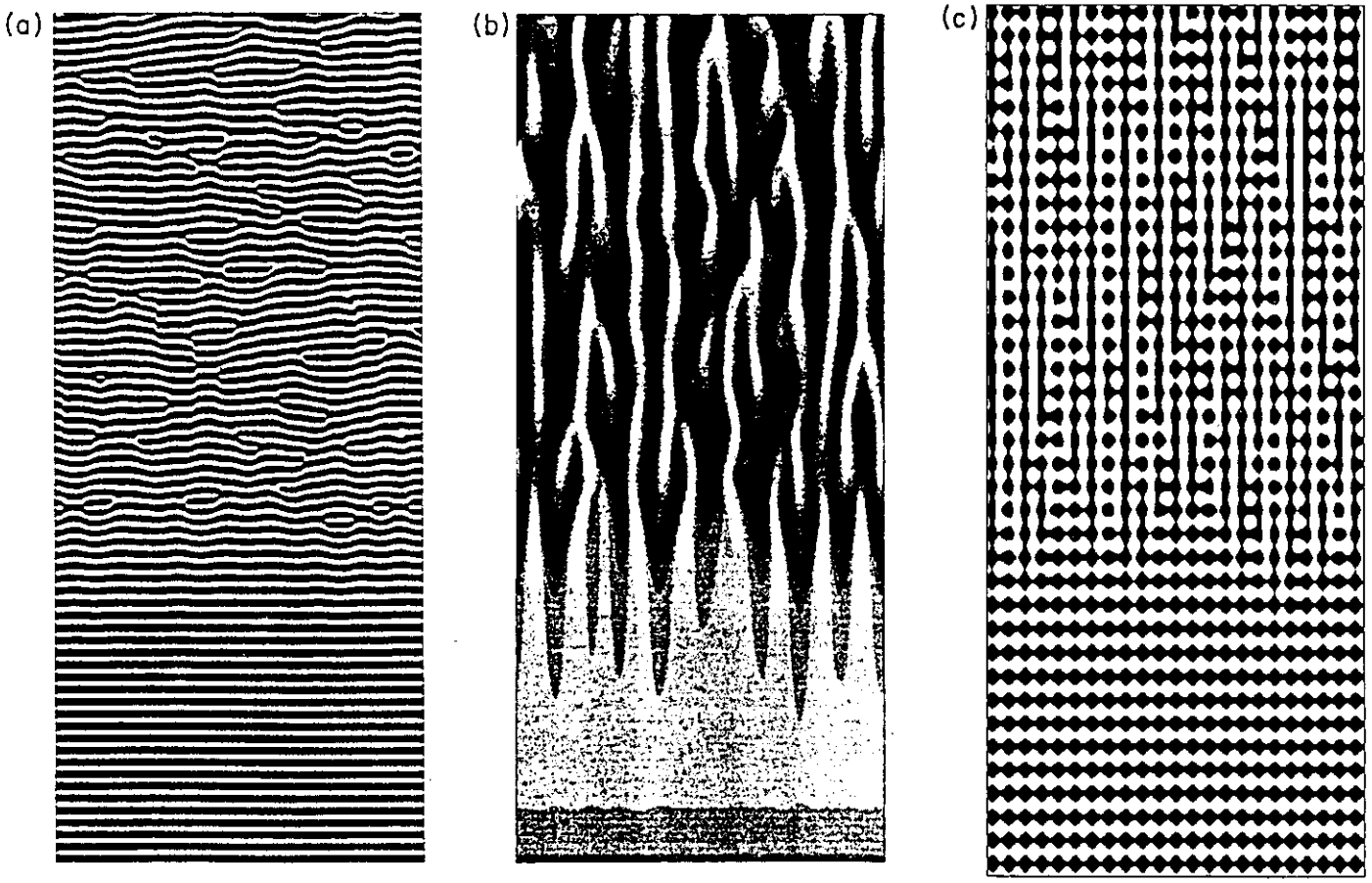

FIG. 1. Space-time plots representing the evolution in a 1D box of length 512 during 700 units of time (running upwards). We bring a stable mixed mode in the region of instability toward defect chaos. The parameters are $\mu_H = 0.3, \mu_T = 0.5, g = 2, \lambda = 1.5, \beta_r = \delta_r = D_T = D_r^H = 1$. We take $D_i^H = 5, \beta_i = 1.6, \delta_i = 3$. Highest values are in white. (a) Lines of constant phase of the Hopf mode. Spatiotemporal defects of phase appear at the points where the amplitude of the Hopf mode locally reaches zero. (b) Amplitude of the Hopf mode. (c) Concentration $\mathbf{c}$ reconstructed as $Te^{i0.28x} + He^{i0.33t} + \text{c.c.}$ We recognize in the first third of time the "polygonal" space-time pattern characteristic of a mixed mode.

tion c is periodic both in space and time leading to a "polygonal" space-time pattern characteristic of a mixed mode [Fig. 1(c)]. In the second part of the time, the defect chaos regime exhibits on the contrary space-time phase dislocations appearing when the amplitude of the Hopf mode locally reaches zero. On the other hand, in the phase chaos regime the amplitudes of the Turing and Hopf modes are fluctuating around their stationary value because the phase of the Hopf solution is turbulent. This weak type of chaos cannot be clearly distinguished on space-time plots from the stable mixed mode, because, though the phase fluctuates, lines of constant phase remain continuous. This phase chaos dynamics is therefore not represented in the figure.

We have studied the transition between the two forms of turbulence by plotting the absolute minimum of the amplitude of the Hopf mode $H_{\min}$ in a given space-time area versus β_i or δ_i. This method clearly distinguishes between transitions of first and second order. In this latter case, the transition between phase and defect chaos is continuous like in the conditions of Fig. 2(a). On the contrary, for first-order transitions there is a hysteresis phenomenon characteristic of bistability between phase and defect chaos [Fig. 2(b)]. We use these graphs to determine the transition points between both regimes. The behavior of the system is then considered for different sets of parameters. In the (δ_i, β_i) plane, the transition between phase and defect chaos appears to be always discontinuous, leading to a hysteretic behavior, as summarized in Fig. 3(a). On the contrary, in the (D_i^H, β_i) plane, both first- and second-order transitions can be observed [Fig. 3(b)]. Moreover, the defect chaos regime may persist in the stable region of this plane where it

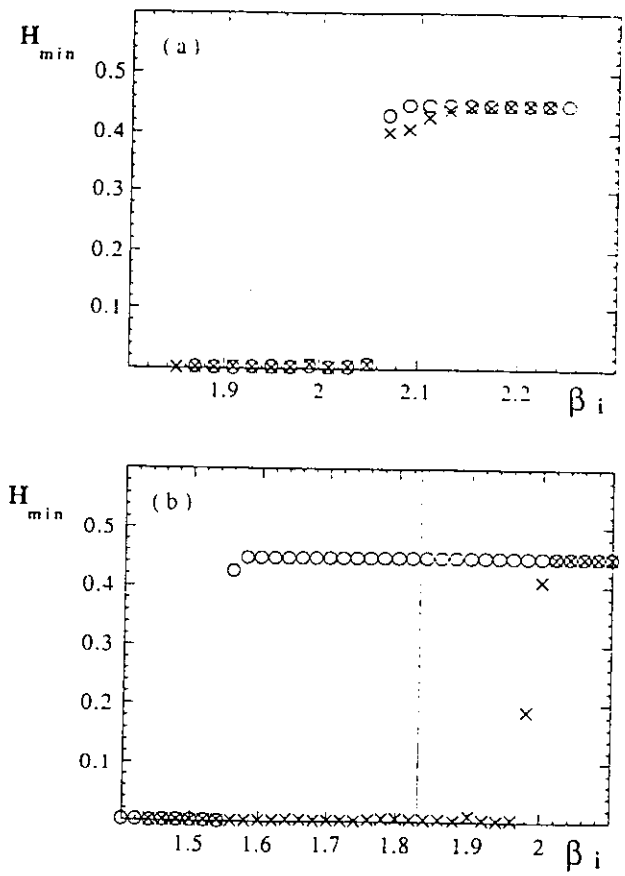

FIG. 2. Minimum of the amplitude of the Hopf mode $H_{\min}$ vs parameter β_i. Following a delay of 3000 units of time after a quasistatic increase (crosses) or decrease (circles) of β_i, $H_{\min}$ is determined in a space-time area of 512 × 500. The solid line stands for the stability limit of the mixed mode [Eq. (7)]. (a) $D_i^H = 4$. Continuous bifurcation characteristic of a second-order transition; (b) $D_i^H = 0.6$. Hysteresis typical of a first-order transition. Below the stability limit of the mixed mode ($\beta_i = 1.83$), defect chaos coexists with the phase chaos regime. For $\beta_i > 1.83$, defect chaos coexists with the stable mixed mode. Note that the measure of $H_{\min}$ is not a good means to distinguish a stable mixed mode from phase chaos of the mixed mode. All other parameters are the same as in Fig. 1.

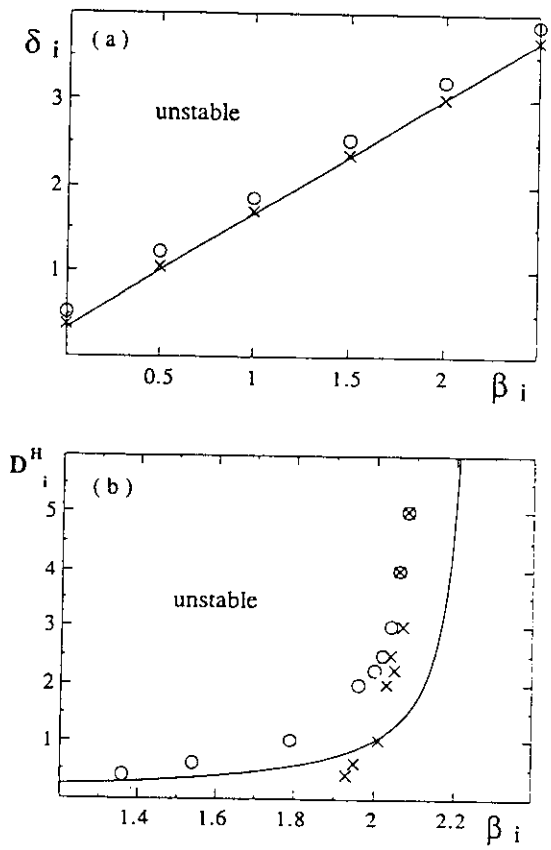

FIG. 3. Phase planes (δ_i, β_i) and (D_i^H, β_i) summarizing the region of stability of the phase and defect chaos. The solid line corresponds to the limit of stability of the Turing-Hopf mixed mode [Eq. (7)]. (a) (δ_i, β_i) plane for $D_i^H = 1$. Crosses stand for the lower limit of stability of the defect chaos regime when δ_i is decreased, while circles represent the upper limit of stability of the phase chaos dynamics when δ_i is increased. The transition between phase and defect chaos regimes is hysteretic (bichaos). (b) (D_i^H, β_i) plane for $\delta_i = 3$. Crosses stand for the upper limit of stability of the defect chaos regime when β_i is increased, while circles represent the lower limit of stability of the phase chaos dynamics when β_i is decreased. Transitions of second order between the two regimes are observed for higher D_i^H's. For lower D_i^H's, the transition is of first order (bichaos). Moreover, defect chaos may persist in the region where the mixed mode is stable. All other parameters are the same as in Fig. 1.

thus coexists with the stable mixed mode [Figs. 2(b) and 3(b)].

We have shown that the mixed modes resulting from the interaction between Turing and Hopf modes may become unstable toward diffusion-induced phase instabilities. This bifurcation gives rise to weak and strong spatiotemporal chaos in the sense that two different regimes of phase and defect chaos are observed. This behavior is reminiscent of the dynamics of the one-dimensional complex Ginzburg-Landau equation beyond the Benjamin-Feir instability [4]. Its origin lies however genuinely in the coupling between Turing and Hopf modes. Indeed, for the values of parameters we have chosen, the complex Ginzburg-Landau equation alone [i.e., Eq. (3) with $\delta_r = \delta_i = 0$] does not exhibit a Benjamin-Feir instability. However, when it is coupled with the amplitude equation for the Turing pattern, the corresponding mixed mode may undergo a phase instability as shown here. From a theoretical point of view, one may test these two phase instabilities to determine if the characteristics of chaotic behaviors may be described in terms of similar universal laws and properties. Moreover, this new mechanism offers another scenario for the onset of spatiotemporal chaos in all degenerate systems where two instabilities breaking, respectively, spatial and temporal symmetry interact. Experimentally, this may be relevant to recent experimental observations in gas discharge [18] and chemical [9] systems. In the latter case, the Turing patterns obtained in the chlorite-iodide–malonic acid (CIMA) reaction arise because the activator species forms a complex of low mobility with starch, the color indicator of the reaction [19]. This gives rise to the difference between the effective mobilities of the reactants necessary to shift a competing Hopf bifurcation so that the Turing structures may exist. When this complex formation effect is progressively relaxed, the shift fades away and both bifurcations start interacting. It is in this transition region that the complex spatiotemporal behaviors have been observed. In this regard, the study of spatiotemporal chaos in a chemical reaction-diffusion model has also been undertaken.

We thank P. Coullet, P. De Kepper, P. Gaspard, G. Nicolis, and A. Pumir for stimulating discussions. P.B. and G.D. received support from the FNRS (Belgium) and A.D. received support from IRSIA (Belgium). This work was supported by the EC Science Program (Twinning No. SC1-CT91-0760).

[1] See *Nonlinear Evolution of Spatio-Temporal Structures in Dissipative Continuous Systems*, edited by F. Busse and L. Kramer (Plenum, New York, 1992).
[2] Y. Kuramoto, *Chemical Oscillations, Waves and Turbulence* (Springer, Tokyo, 1984).
[3] P. Coullet, L. Gil, and J. Lega, Phys. Rev. Lett. **62**, 1619 (1989).
[4] B.I. Shraiman, A. Pumir, W. van Saarloos, P.C. Hohenberg, H. Chaté, and M. Holen, Physica D **57**, 241 (1992).
[5] A. Turing, Philos. Trans. R. Soc. London Ser. B **237**, 37 (1952).
[6] V. Castets, E. Dulos, J. Boissonade, and P. De Kepper, Phys. Rev. Lett. **64**, 2953 (1990).
[7] Q. Ouyang and H.L. Swinney, Nature **352**, 610 (1991).
[8] Q. Ouyang and H.L. Swinney, Chaos **1**, 411 (1991).
[9] J.-J. Perraud, K. Agladze, E. Dulos, and P. De Kepper, Physica A **188**, 1 (1992).
[10] Y.X. Li, Phys. Lett. A **147**, 204 (1990).
[11] H. Kidachi, Progr. Theor. Phys. **63**, 1152 (1980).
[12] J.P. Keener, Stud. Appl. Math. **55**, 187 (1976).
[13] J. Guckenheimer and P. Holmes, *Nonlinear Oscillations, Dynamical Systems and Bifurcations of Vector Fields* (Springer-Verlag, Berlin, 1983).
[14] J.-J. Perraud, A. De Wit, E. Dulos, P. De Kepper, G. Dewel, and P. Borckmans, Phys. Rev. Lett. **71**, 1272 (1993).
[15] Y. Kuramoto, Suppl. Progr. Theor. Phys. **64**, 346 (1978).
[16] G.I. Sivashinsky, Acta Astron. **6**, 569 (1979).
[17] H. Sakaguchi, Progr. Theor. Phys. **84**, 792 (1990).
[18] H. Willebrand, F.-J. Niedernostheide, R. Dohmen, and H.-G. Purwins, in *Oscillations and Morphogenesis*, edited by L. Rensing (Dekker, New York, 1993), p. 81.
[19] I. Lengyel and I.R. Epstein, Proc. Natl. Acad. Sci. USA **89**, 3977 (1992).

Chaotic spatially subharmonic oscillations

D. Lima, A. De Wit,* G. Dewel, and P. Borckmans
Service de Chimie Physique and Centre for Nonlinear Phenomena and Complex Systems, Code Postal 231, Université Libre de Bruxelles, Campus Plaine, 1050 Brussels, Belgium
(Received 5 October 1995)

The interplay between two instabilities respectively breaking space and time symmetries can give rise to spatially subharmonic oscillations generated by a self-induced parametric instability. In one-dimensional systems, the resulting dynamics consists in a pattern with two wave numbers oscillating with one frequency. Conditions are given for which this solution becomes phase unstable giving rise to spatiotemporal chaos.

PACS number(s): 05.45.+b, 47.20.Ky

A rich variety of complex spatiotemporal behaviors may occur in the vicinity of multiple bifurcation points [1]. In particular, the interaction between a steady instability that breaks spatial symmetry and a bifurcation breaking time translation symmetry has been the subject of numerous studies [2–7]. As an example, we have reported previously that the interplay between the Turing and Hopf instabilities can give rise to localized structures in the form of asynchronous wave sources with structured cores [8] or to a chaotic Turing-Hopf mixed mode [9]. Such dynamical behaviors have now been observed experimentally in a chemical system [8,10]. In this Rapid Communication, we show that self-induced subharmonic bifurcations can also be generated by resonances near such degenerate instability points. In some cases, the resulting subharmonic dynamics can become spatiotemporally chaotic.

We suppose that the reference homogeneous steady state (HSS) of a one-dimensional (1D) physicochemical system can undergo both a pattern-forming instability giving rise to a periodic structure with a wavelength $\lambda_c = 2\pi/q_c$ and a Hopf bifurcation. The distance between the two thresholds of instability, the unfolding parameter, is denoted as δ. For example, in the case of chemical reactions taking place in a gel, the concentration of the color indicator immobilized in the matrix allows one to control the distance between the Turing and Hopf bifurcation points [8,10]. If δ is sufficiently small, the eigenvalue of the 1/2 subharmonic of the steady critical mode can become complex and near the critical point the corresponding real part is small. The resonant interaction between the corresponding pair of Hopf modes with wave number $q_c/2$ and the steady state with wave number q_c must then be taken into account [11]. In the vicinity of such a critical situation, the field variable of the problem $\underline{C}(x,t)$ may be expressed in terms of the steady mode with amplitude T and two traveling waves with amplitudes A_R and A_L:

$$\underline{C}(x,t) = \underline{C}_0 + Te^{iq_c x}\underline{e}_T + A_L e^{i[\omega(q_c/2)t - q_c x/2]}\underline{e}_L + A_R e^{i[\omega(q_c/2)t - q_c x/2]}\underline{e}_R + \text{c.c.} \tag{1}$$

where $\underline{C}_0$ is the reference HSS, $\underline{e}_T$, $\underline{e}_L$, and $\underline{e}_R$ the critical eigenvectors of the linearized matrix corresponding to the steady state and the Hopf modes while $\omega(q_c/2)$ is the critical frequency of the Hopf mode with wave number $q_c/2$. The competition between these modes is then described by amplitude equations that are derived by the use of standard techniques [12,13]. If τ and χ are the slow time and space scales then

$$\frac{\partial T}{\partial \tau} = \mu_T T - g|T|^2 T - \lambda(|A_R|^2 + |A_L|^2)T + \upsilon A_R^* A_L + D\frac{\partial^2 T}{\partial \chi^2}, \tag{2}$$

$$\frac{\partial A_R}{\partial \tau} = \mu' A_R - g'|A_R|^2 A_R - h'|A_L|^2 A_R - \lambda'|T|^2 A_R + \upsilon' T^* A_L - c\frac{\partial A_R}{\partial \chi} + D'\frac{\partial^2 A_R}{\partial \chi^2}, \tag{3}$$

$$\frac{\partial A_L}{\partial \tau} = \mu' A_L - g'|A_L|^2 A_L - h'|A_R|^2 A_L - \lambda'|T|^2 A_L + \upsilon' T A_R + c\frac{\partial A_L}{\partial \chi} + D'\frac{\partial^2 A_L}{\partial \chi^2}. \tag{4}$$

The coupling constants appearing in these equations can be related to the parameters of the system. The primed coefficients are complex ($\alpha' = \alpha_r' + i\alpha_i'$) while $\mu_r' = \mu_T + \delta$ where μ_T measures the distance from the steady bifurcation threshold and c is related to the group velocity of the waves. The most important feature of the above equations is the presence of a resonant interaction proportional to υ and υ' induced by the coupling between the steady mode and the waves. This term introduces a phase dependence into the dynamics. The simplest nontrivial solution of these equations is a pure steady state:

$$T^2 = \frac{\mu_T}{g}, \quad A_R = A_L = 0. \tag{5}$$

It is the first to appear supercritically when $\delta < 0$ and $g > 0$. As the bifurcation parameter μ_T is increased above zero, this periodic structure undergoes an instability for $\mu_T = \mu_I$ where μ_I is determined from

*Electronic address: adewit@ulb.ac.be

1063-651X/96/53(2)/1305(4)/$06.00

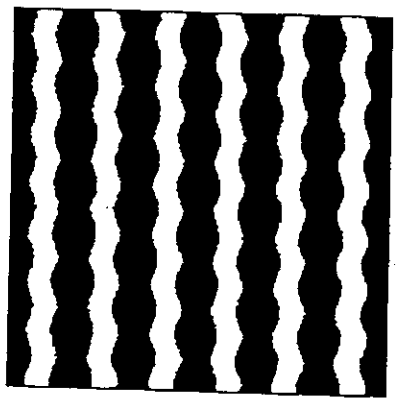

FIG. 1. Space-time density plot of $C(x,t)$ showing the stable subharmonic mixed mode. The amplitudes T, A_R, and A_L have been obtained by integrating the system (2)–(4) without diffusion and group velocity using an explicit Euler scheme. The parameters are $\mu_T=0.7$, $g=2$, $\lambda=4$, $v=1$, $\delta=-0.05$, $g'=3+i$, $h'=6+i$, $\lambda'=2+i$, $v'=0.2+0.5i$. The field variable is then reconstructed as $C(x,t)=Te^{i(0.4x}+A_Le^{i(0.1t-0.2x)}+A_Re^{i(0.1t-0.2x)}+\text{c.c.}$ The minima (maxima) of $C(x,t)$ are in white (black). Time is running downwards.

$$\mu_I+\delta-\lambda_r'(\mu_I/g)+v_r'\sqrt{\mu_I/g}=0 \tag{6}$$

obtained through a linear stability analysis. When the following condition is satisfied:

$$2(g_r'+h_r')\mu_I-[v_r-2\lambda_r\sqrt{\mu_I/g}][v_r'-2\lambda_r'\sqrt{\mu_I/g}]>0, \tag{7}$$

the solution that bifurcates from the pure steady state mode at $\mu_T=\mu_I$ corresponds to a mixed mode for which

$$T=T_M, \quad A_R=R_Me^{i[\Omega_M t-\phi_R]}, \quad A_L=R_Me^{i[\Omega_M t-\phi_L]}. \tag{8}$$

By an appropriate choice of the origin of coordinates, we can consider T_M as real. When $v_r'>0$, the phase dynamics implies that

$$\phi_R=\phi_L. \tag{9}$$

Substituting into Eqs. (2)–(4), and equating real and imaginary parts, we get

$$\Omega_M=\mu_i'-R_M^2[g_i'+h_i']-\lambda_i'T_M^2+v_i'T_M, \tag{10}$$

$$R_M^2=\frac{\mu_r'-\lambda_r'T_M^2+v_r'T_M}{[g_r'+h_r']}, \tag{11}$$

$$0=[\mu_T-2\lambda R_M^2]T_M+vR_M^2-gT_M^3. \tag{12}$$

The spatiotemporal dynamics corresponding to this mixed mode solution is thus the combination of a steady structure with wavelength q_c and a standing wave formed by the superposition of the left- and right-going waves ($A_R=A_L$) with wave number $q_c/2$ and frequency $\omega(q_c/2)$. The corresponding space-time plot for the reconstructed field $C(x,t)$[Eq. (1)] is displayed in Fig. 1. The characteristic polygonal space-time structure of a mixed mode is obtained. At each location, the system is oscillating with one frequency but, because of the presence of two wave numbers, we see that the minima of the structure are shifted one wavelength every half period of oscillation. This dynamical behavior presents strong analogies with the spatially subharmonic oscillations

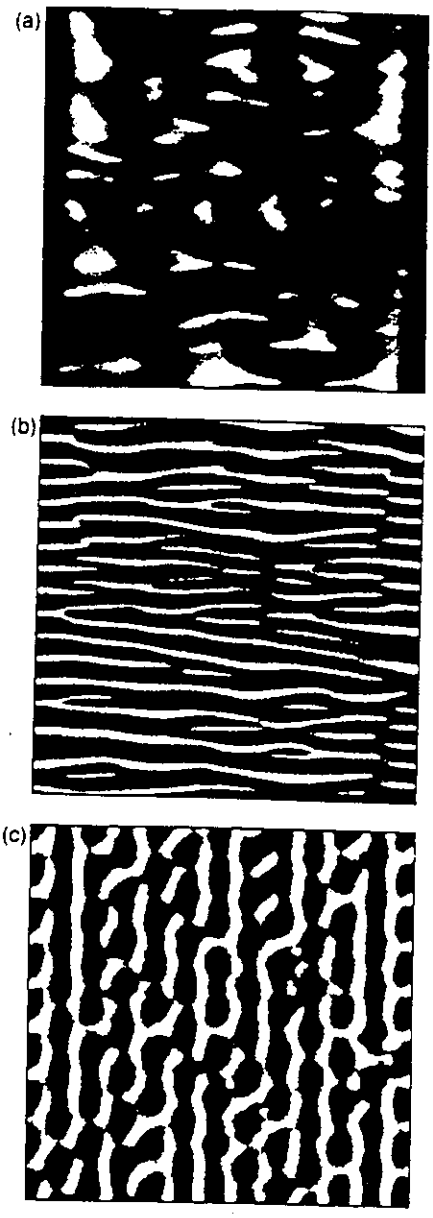

FIG. 2. Space-time density plots of the spatiotemporal chaos obtained when the subharmonic mixed mode is phase unstable. Integration of the amplitude equations (2)–(4) is performed with diffusion and group velocity on a system of length 64 during 120 units of time using periodic boundary conditions. The spatial differentiation has been made using finite differences. All conditions are the same as in Fig. 1 except $g'=3.0+0.2i$, $\lambda'=2+5i$, $D=0$, $D'=0.5+5i$ while $c=0.01$. (a) and (b) amplitude and phase of the right-going wave shown on scales τ and χ; (c) field variable $C(x,t)=Te^{i0.3x}+A_Le^{i(0.1t+1.5x)}+A_Re^{i(0.1t-1.5x)}+\text{c.c.}$ reconstructed on scales t and x.

that have been observed on the 1D front in the flow of a fluid inside a partially filled rotating horizontal cylinder [14]. Similar oscillating patterns have also been obtained in numerical integration of a reaction-diffusion model in the vicinity of the codimension-two Turing-Hopf point [15]. These mixed modes are of a different origin than those introduced in [4]. It is worthwhile to point out that for the values of the parameters used in Fig. 1, the standing wave of the system [(3) and (4)] with $T=0$ are unstable versus traveling waves ($h_r'>g_r'$). It is known that such a standing wave can be stabilized if an external time modulation with a frequency twice the frequency of the traveling waves is applied to the system [16,17]. Here we show that the stabilization of the standing waves can also be self-induced by an intrinsic coupling with the steady mode which plays the role of an external forcing by restoring the left-right symmetry.

The mixed mode [Eq. (8)] is stable versus spatially uniform amplitude perturbations as long as the following inequalities are satisfied:

$$\Delta=[g_r'+h_r']\left[2gT_M^2+\frac{vR_M^2}{T_M}\right]-[v_r'-2\lambda_r'T_M][v-2\lambda T_M]>0, \tag{13}$$

$$Tr=-\left[2(g_r'+h_r')R_M^2+2gT_M^2+\frac{vR_M^2}{T_M}\right]<0. \tag{14}$$

However, in the experiments on 1D fronts [14], when the bifurcation parameter is increased beyond μ_I, spatial modulations appear spontaneously which disturb the regularity of this oscillating subharmonic pattern. It is thus necessary to study also the stability of the mixed mode with respect to inhomogeneous perturbations. The mixed mode solution [Eq. (8)] is invariant under the transformation

$$\psi(T, A_L, A_R)=(T, e^{i\psi}A_L, e^{i\psi}A_R) \tag{15}$$

which corresponds to a shift in time $t'\rightarrow t-\psi/\Omega_M$. This property generates a whole family of solutions and induces a zero eigenvalue in the homogeneous linearized matrix. In the presence of slow spatial modulations that preserve the condition (9) on the large scales, $\psi(x,t)$ depends on space and time and obeys a phase diffusion equation of the form [12]

$$\frac{\partial\psi}{\partial t}=\mathcal{D}\frac{\partial^2\psi}{\partial x^2}+\kappa\left(\frac{\partial\psi}{\partial x}\right)^2. \tag{16}$$

A phase instability occurs when $\mathcal{D}=0$. After a little algebra, it is easy to show that this long wavelength instability takes place when

$$\mathcal{D}=D_r'+\frac{D_i'}{\Delta}\left\{[g_i'+h_i']\left[2gT_M^2+\frac{vR_M^2}{T_M}\right]-[v_i'-2\lambda_i'T_M][v-2\lambda T_M]\right\}<0. \tag{17}$$

This condition is the analog for the subharmonic mixed mode of the Benjamin-Feir stability criterion for the traveling waves [12]. We have numerically integrated the amplitude equations (2)–(4) for values of parameters that satisfy the condition (17). In the case presented here, the resulting phase instability spontaneously generates numerous phase defects [18] and large fluctuations of the three amplitudes thus mediating spatiotemporal chaos as shown in Fig. 2. When the amplitude of the waves locally reaches zero [white regions in Fig. 2(a)], the phase of the waves exhibits space-time dislocations [Fig. 2(b)], a behavior reminiscent of the so-called "amplitude chaos" [18,19]. The space-time plot of the reconstructed field variable $\underline{C}(x,t)$ confirms that the system does not oscillate at the locations where the amplitude of the waves is minimum thus expressing the steady state solution. On the contrary, when the amplitude of the waves is maximum, the amplitude of the steady state is minimum and the system is locally in an oscillating mode.

As long as the phase difference is locked on the large scale, i.e., condition (9) is fulfilled, the resonant interaction plays a crucial role in the localization of the defects [17]. However, when the group velocity is sufficiently large, the state with $\Phi=\phi_R-\phi_L=0$ is destabilized. The phase variable Φ then obeys a sine-Gordon equation of diffusion type that is known to admit stable propagating solitons as solutions [20,21]. Such solitary waves have also been observed in the film draining experiment [22].

In this Rapid Communication, we have shown that the coupling between a pattern-forming instability and a Hopf instability can induce a bifurcation from a steady pattern towards a subharmonic structure characterized by two wave numbers and one frequency. We have next given the conditions under which this subharmonic pattern can become phase unstable giving rise to a spatiotemporally chaotic dynamics. This scenario explains the sequence of bifurcations recently observed experimentally in a hydrodynamical system [14]. Such a scenario should also exist in chemical systems where the degeneracy between the Turing and Hopf instabilities can be achieved experimentally. The subharmonic pattern has indeed been observed in the numerical integration of the reaction-diffusion Brusselator model near the codimension-two Turing-Hopf point [15]. Let us furthermore note that subharmonic patterns have also been obtained in a study of two different immiscible liquids lying in layers between horizontal walls and heated from below [23]. Finally, a parametric instability of a homogeneous limit cycle towards a subharmonic mixed mode with two wave numbers and two frequencies followed by a transition to spatiotemporal chaos has also been documented recently in the Brusselator model [15] and in the Gray-Scott model [24]. In the latter case, the stabilization of the spatiotemporal chaos has allowed one to track an unstable Turing pattern. These results emphasize the need to understand in detail the mechanisms of appearance of spatiotemporal chaos near degenerate bifurcation points.

D.L. thanks the CNPQ (Brazil) for its financial support. A.D., G.D., and P.B. acknowledge financial help from the F.N.R.S. (Belgium).

[1] J. Guckenheimer and P. Holmes, *Nonlinear Oscillations, Dynamical Systems, and Bifurcations of Vector Fields* (Springer Verlag, New York, 1983).
[2] J.P. Keener, Stud. Appl. Math. **55**, 187 (1976).
[3] H. Kidachi, Prog. Theor. Phys. **63**, 1152 (1980).
[4] B.J.A Zielinska, D. Mukamel, and V. Steinberg, Phys. Rev. A **33**, 1454 (1986), and references therein.
[5] W. Zimmermann, D. Armbruster, L. Kramer, and W. Kuang, Europhys. Lett. **6**, 505 (1988) and references therein.
[6] P. Kolodner, Phys. Rev. E **48**, R665 (1993).
[7] G. Heidemann, M. Bode, and H.-G. Purwins, Phys. Lett. A **177**, 225 (1993).
[8] J.-J. Perraud, A. De Wit, E. Dulos, P. De Kepper, G. Dewel, and P. Borckmans, Phys. Rev. Lett. **71**, 1272 (1993).
[9] A. De Wit, G. Dewel, and P. Borckmans, Phys. Rev. E **48**, R4191 (1993).
[10] P. De Kepper, J.-J. Perraud, B. Rudovics, and E. Dulos, Int. J. Bif. Chaos **4**, 1215 (1994).
[11] A. Hill, and I. Stewart, Dynam. Stab. Syst. **6**, 149 (1991).
[12] M.C. Cross and P.C. Hohenberg, Rev. Mod. Phys. **65**, 851 (1993).
[13] M. Cheng and H.-C. Chang, Phys. Fluids A **4**, 505 (1992).
[14] D.P. Vallette, W.S. Edwards, and J.P. Gollub, Phys. Rev. E **49** R4783 (1994).
[15] A. De Wit, Ph.D. thesis, Université Libre de Bruxelles, 199[illegible] (unpublished).
[16] H. Riecke, J.D. Crawford, and E. Knobloch, Phys. Rev. Lett **61**, 1942 (1988).
[17] P. Coullet, K. Emilsson, and D. Walgraef, Physica D **61**, 1[illegible] (1992).
[18] P. Coullet, L. Gil, and J. Lega, Phys. Rev. Lett. **62**, 161[illegible] (1989).
[19] B.I. Shraiman, A. Pumir, W. van Saarloos, P.C. Hohenberg, H Chaté, and M. Holen, Physica D **57**, 241 (1992).
[20] M. Büttiker and R. Landauer, Phys. Rev. A **23**, 1397 (1981).
[21] Y. Tegami, Physica D **21**, 325 (1986).
[22] F. Melo and S. Douady, Phys. Rev. Lett. **71**, 3283 (1993).
[23] K. Fujimura and Y. Renardy, Physica D **85**, 25 (1995).
[24] V. Petrov, S. Métens, P. Borckmans, G. Dewel, and K. Showalter, Phys. Rev. Lett. **75**, 2895 (1995).

Spatiotemporal dynamics near a codimension-two point

A. De Wit,* D. Lima, G. Dewel, P. Borckmans
Service de Chimie Physique, Centre for Nonlinear Phenomena and Complex Systems and Nonlinear Chemistry Unit, Case Postal 231, Université Libre de Bruxelles, Campus Plaine, 1050 Brussels, Belgium
(Received 25 January 1996)

Spatiotemporal dynamics resulting from the interaction of two instabilities breaking, respectively, spatial and temporal symmetries are studied in the framework of the amplitude equation formalism. The corresponding bifurcation scenarios feature steady-Hopf bistability with corresponding localized structures but also different types of mixed states. Some of these mixed modes result from self-induced subharmonic instabilities of the pure steady and Hopf modes. The bifurcation schemes are then used to organize the results of numerical simulations of a one-dimensional reaction-diffusion model. These dynamics are relevant to experimental chemical systems featuring a codimension-two Turing-Hopf point but also to any experimental setup where homogeneous temporal oscillations and spatial patterns are obtained for nearby values of parameters. [S1063-651X(96)03707-5]

PACS number(s): 05.45.+b, 47.20.Ky

I. INTRODUCTION

In nonequilibrium systems, instabilities breaking either temporal or spatial symmetry have been studied [1] in fields as diverse as hydrodynamics [2], nonlinear optics [3], active chemical systems [4,5], etc. Recently, dynamics resulting from the interaction of both types of instabilities have been observed in several experimental systems [6–13]. Among these, chemical systems have proved to be a generic example as they genuinely present both types of instabilities. On the one hand, oscillating reactions in well mixed reactors have indeed become the typical examples of systems undergoing a Hopf bifurcation resulting from a breaking of time symmetry. On the other hand, the breaking of spatial symmetry in chemical systems is now well documented [4,5] since its observation in the chlorite-iodide-malonic acid (CIMA) reaction in 1990 [14]. The periodic stationary spatial patterns that emerge in that case result from a Turing instability based solely on the coupling between nonlinear chemical reactions and molecular diffusion [15]. A necessary condition for the Turing instability to occur is that the diffusion coefficient of the inhibitor species should be sufficiently larger than that of the activator. In the experiments, color indicators are used to visualize the patterns. They consist of large molecular weight molecules of very small (in the gel possibly zero) diffusivity. Such color indicators act to create favorable conditions to the formation of Turing structures because they bind to the activator species thereby reducing its effective mobility [16]. For a low indicator concentration, waves characteristic of a Hopf oscillating regime are observed while Turing patterns take over for higher concentrations of the indicator. This one therefore controls the distance between the thresholds of the Turing and Hopf instabilities that coincide at a codimension-two Turing-Hopf point (CTHP). Changing the concentration of malonic acid allows one to scan the bifurcation scenario near this point. In the vicinity of this degenerate point, a wealth of complex spatiotemporal dynamics are observed. The ideas that will be discussed below in the chemical context are of greater generality as a CTHP can be expected to occur in any other experimental setup where two instabilities breaking, respectively, spatial and temporal symmetries interact. The mechanism giving rise to the spatial pattern is then not necessarily the chemical Turing instability.

Formally, a CTHP point is obtained when the linear stability analysis of a reference homogeneous steady state features a degeneracy between a real root vanishing for a wave number k_c and a pair of complex conjugated roots with frequency ω_c that both have a zero real part. Then the real root corresponds to a stationary spatial Turing pattern characterized by the wave-number–frequency couple $(k_c,0)$ while the complex roots relates to the Hopf mode $(0,\omega_c)$ corresponding to a temporal oscillation with frequency ω_c. Let us consider the conditions to obtain a CTHP in the reaction-diffusion Brusselator model. This model was chosen because it has already been the subject of extensive analytical and numerical studies related to both single Turing and Hopf instabilities [17,18]. The evolution equations of the Brusselator model read

$$\partial_t X = A-(B+1)X+X^2Y+D_x\nabla^2 X,$$

$$\partial_t Y = BX-X^2Y+D_y\nabla^2 Y. \tag{1}$$

The concentration of species B is chosen as the bifurcation parameter. The homogeneous steady state $(X_s,Y_s)=(A,B/A)$ of system (1) undergoes a Turing instability when $B>B_c^T=(1+A\sqrt{D_x/D_y})^2$. A stationary spatial pattern then emerges characterized by an intrinsic critical wave vector $k_c^2=A/\sqrt{D_xD_y}$. The steady state may also go through a Hopf instability if $B>B_c^H=1+A^2$, evolving then into a homogeneous limit cycle characterized by a critical frequency $\omega_c=A$. The thresholds of these two instabilities coincide at the CTHP point such that $B_c=B_c^H=B_c^T$. This

*Electronic address: adewit@ulb.ac.be

condition is achieved when the ratio of the diffusion coefficients $\sigma = D_x/D_y$ reaches its critical value $\sigma_c = [(\sqrt{1+A^2}-1)/A]^2$.

In this work we study the bifurcation scenarios that can be obtained in one-dimensional systems near the CTHP. Previous analyses [19–22] have tackled this problem and classified the bifurcation scenarios, focusing on the interaction between the steady mode and the Hopf mode without taking into account spatial effects or subharmonic bifurcations of the basic modes. However, by numerically integrating the Brusselator model for values of parameters near a CTHP, we have discovered several spatiotemporal dynamics that do not enter the previously obtained classes of bifurcation scenarios. We will consider here only a two-variable model excluding the possibility of oscillating behavior and waves originating through a Hopf bifurcation with finite wave number. The aim of this work is to extend the previous studies of the Turing-Hopf interaction by reviewing the different spatiotemporal dynamics that can be observed near a CTHP. To do so, we compare the theoretical bifurcation schemes derived in the framework of amplitude equations to the peculiarities obtained by the numerical integration of the Brusselator. The resulting dynamics that can be observed near a CTHP can be divided into two main groups. The first one gathers the dynamics due to the interaction between a Turing mode and a Hopf mode. Their interplay can give rise to bistability, localized structures, and to a mixed mode as is discussed in Sec. II. The second group of spatiotemporal dynamics results from subharmonic instabilities of either the Turing or the Hopf mode and features more complex mixed modes. Sections III and IV are, respectively, devoted to the subharmonic instability of the Turing and the Hopf modes. Section V discusses additional spatiotemporal scenarios observed in the reaction-diffusion model before we summarize and conclude in Sec. VI.

II. INTERACTION BETWEEN A TURING MODE AND A HOPF MODE

The CTHP is characterized by the fact that three roots of the characteristic equation of the linear stability analysis have their real part which vanishes simultaneously. As an example, in the Brusselator model and for a given value of A, this occurs at the critical point (B_c, σ_c). In the vicinity of such a degenerate point, a Turing mode $T(k_c,0)$ with wave number k_c interacts with a homogeneous Hopf mode $H(0,\omega_c)$ with frequency ω_c. For one-dimensional systems, the variables C of the system can be described by a superposition of these two modes:

$$\mathbf{C}(x,t) = \mathbf{C}_0 + T e^{ik_c x}\mathbf{w}_T + H e^{i\omega_c t}\mathbf{w}_H + \text{c.c.} \qquad (2)$$

$\mathbf{C}_0$ is the uniform reference state whereas $\mathbf{w}_T$ and $\mathbf{w}_H$ are the critical eigenvectors of the Turing and Hopf linearized evolution operator, while c.c. stands for complex conjugate. T and H are the amplitudes of the spatial and temporal modulations, respectively. The competition between these two modes is then described by the coupled amplitude equations [19,21,22]:

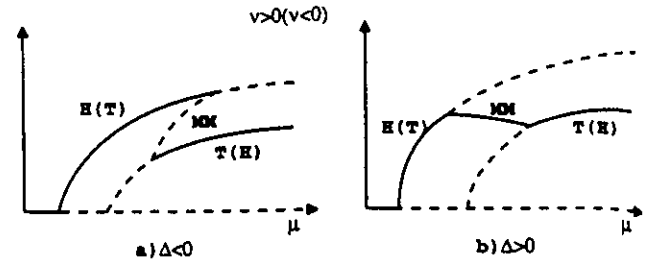

FIG. 1. Theoretical bifurcation diagrams when a Turing mode interacts with a Hopf mode. Solid and dashed lines correspond to stable and unstable states, respectively. (a) When $\Delta<0$, we get bistability between the Turing and Hopf modes. If $\nu>0$, we have the succession Hopf-bistability-Turing (H-B-T) and the inverse sequence T-B-H when $\nu<0$. (b) When $\Delta>0$, a stable mixed mode is observed. If $\nu>0$, we have the succession H-MM-T and the inverse sequence T-MM-H when $\nu<0$.

$$\frac{\partial T}{\partial t} = \mu T - g|T|^2 T - \lambda |H|^2 T, \qquad (3)$$

$$\frac{\partial H}{\partial t} = \mu_H H - (\beta_r + i\beta_i)|H|^2 H - (\delta_r + i\delta_i)|T|^2 H, \qquad (4)$$

where μ and $\mu_H = \mu + \nu$ are the two unfolding parameters, ν being the distance between the two thresholds of instability which vanishes at the codimension-two point. In the Brusselator, when $\sigma > \sigma_c$, the Hopf instability occurs before the Turing one and hence $\nu>0$. On the contrary when $\sigma<\sigma_c$, the first instability to occur is the Turing one and in that case $\nu<0$. We will suppose that λ and δ_r are positive as well as g and β_r, this last condition ensuring that the two bifurcations will be supercritical. Notice that for the Brusselator, β_r is always positive. The slow spatial dependence should be introduced if secondary instabilities with long wavelength are to be studied. The system (3) and (4) possesses three nontrivial global solutions: (1) a Turing structure: $T = \{\mu/g\}^{1/2}$, $H=0$; (2) a homogeneous limit cycle: $T=0$, $H = \{\mu_H/\beta_r\}^{1/2} e^{i\Omega t}$ with the renormalization frequency $\Omega = -\beta_i \mu_H/\beta_r$; and (3) a mixed mode (MM): $T = \{[\beta_r\mu - \lambda\mu_H]/\Delta\}^{1/2}$, $H = \{[g\mu_H - \delta_r\mu]/\Delta\}^{1/2} e^{i\Omega_M t}$ with $\Delta = \beta_r g - \lambda\delta_r$ and $\Omega_M = -\beta_i|H_M|^2 - \delta_i|T_M|^2$, where H_M and T_M are the preexponential factors of H and T. This solution corresponds to a Turing pattern with wave number k_c oscillating periodically in time with the frequency $(\omega_c + \Omega_M)$.

Depending on the specific values of the coefficients of Eqs. (3) and (4), the relative stability of these three solutions may vary, leading to different bifurcation scenarios [9,19,21–23].

(i) If $\Delta<0$, the mixed mode is always unstable while the pure Turing and Hopf modes are both stable in a given domain. When $\nu>0$, a regular increase of μ gives successive transitions between the Hopf oscillations, the Turing-Hopf bistability domain, and stationary Turing patterns. This scheme is abbreviated as H-B-T. The inverse sequence T-B-H is obtained when $\nu<0$ [Fig. 1(a)].

(ii) If $\Delta>0$, the mixed mode is stable in the domain where the Turing and Hopf modes are both unstable. When

$\nu>0$, we successively observe, by increasing μ, the homogeneous limit cycle, the Turing-Hopf mixed mode, and stationary Turing patterns, i.e., the sequence H-MM-T and the inverse sequence T-MM-H when $\nu<0$ [Fig. 1(b)]. For some values of parameters, the mixed mode can appear subcritically or also undergo a Hopf bifurcation of its amplitudes T and H [22]. The limit cycle resulting from this instability can disappear through a heteroclinic orbit around which complex spatiotemporal behavior is expected to occur even in small systems.

Near the CTHP, the coupling between the Turing and Hopf instabilities thus allows one to observe different scenarios (Turing-Hopf bistability or a Turing-Hopf mixed mode) depending on the values of the parameters. We will now illustrate these with the one-dimensional Brusselator model numerically integrated by means of an implicit scheme based on finite difference methods. Unless stated otherwise in the captions, all space-time maps presented in this article feature the X variable shown on a gray scale ranging from its minimum (white) to its maximum (black) value. Let us remark that in this model, some nonlinear terms in the equations for the perturbations around the steady state are proportional to the bifurcation parameter B. This characteristic leads to a renormalization of the coefficients [24] of the amplitude equations (3) and (4) proportional to the distance $(B-B_c,\sigma-\sigma_c)$, making the task of linking the bifurcation diagrams of Fig. 1 and those obtained numerically for the Brusselator more difficult. Our simulations of the Brusselator will thus focus on checking qualitatively to what extent the model bifurcation scenarios describe the spatiotemporal dynamics of a system near a CTHP. In particular, we will show effects that have not yet been described in previous work.

A. Bistability and localized structures

In the Turing-Hopf bistability domain, the system evolves, for a given set of parameters, either to homogeneous temporal oscillations of the variables or to a stationary spatial pattern depending on the initial condition. For some values of parameters near the CTHP, both schemes H-B-T and T-B-H are observed numerically in the Brusselator in some subdomains of the parameter space $(A,\sigma/\sigma_c)$. In addition, a stable front between a Turing domain and a train of plane waves [Fig. 2(a)] exists in the bistability domain. The stability of this simplest localized state is related to a nonadiabatic effect due to the interaction of the front with the periodicity of the spatial organization [18,25–29]. This effect which is not contained in the amplitude equation formalism may occur for fronts between two states one of which is periodic in space. It appears, for instance, in the growth of crystals where the interaction between the interface and the periodic structure gives rise to a periodic potential. If the difference in free energy between the two phases is smaller than the energy required to move the front by one wavelength, the front remains pinned. The Brusselator being a nonpotential model, one cannot define a function to minimize near the CTHP. However, the picture of an interaction between the front and the Turing structure remains qualitatively correct and gives rise to an intrinsic pinning of the Turing-Hopf front for a large set of values of the control parameter B (Fig. 3). The nonadiabatic effect also accounts for a stepwise progression of the Turing-Hopf front outside the pinning domain [18,29,30]. In this process, the mode locking phenomenon shows up as a tendency of the average velocity to lock into rational multiples of the Hopf frequency [31]. The sim-

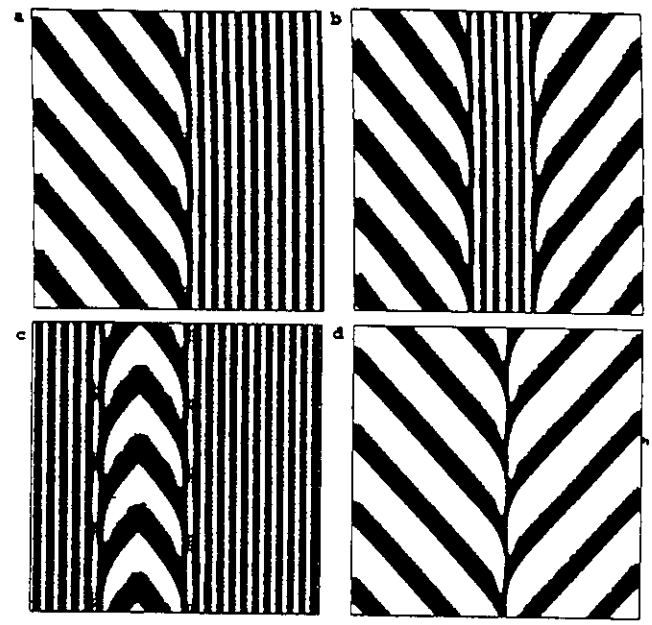

FIG. 2. Space-time maps of localized structures. A one-dimensional Brusselator model of length $L=250$ with no-flux boundary condition (BC) evolves in time running upwards during 20 units of time. The parameters are $A=2.5$, $D_x=4.11$, $D_y=9.73(\sigma/\sigma_c=0.92)$. (a) Turing-Hopf front $(B=10)$. (b) Turing structure embedded in a Hopf background $(B=10)$. (c) Hopf mode embedded in a Turing background $(B=10)$. (d) "Flip-flop" dynamics shown during 50 units of time $(B=12.5)$.

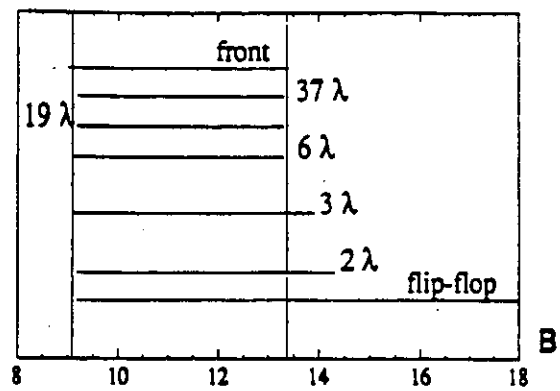

FIG. 3. Stability domain of the different localized structures shown in Fig. 2. The sign $x\lambda$ denotes localized Turing domains containing x wavelengths in their core. For the values of parameters used here, localized Turing domains with down to five wavelengths have the same pinning domain as that of the front which results from a nonadiabatic effect. Localized Turing domains with fewer than five wavelengths have a wider stability domain thanks to the action of a nonvariational effect. The "flip-flop" shown in Fig. 2(d) is the localized structure stable in the largest domain.

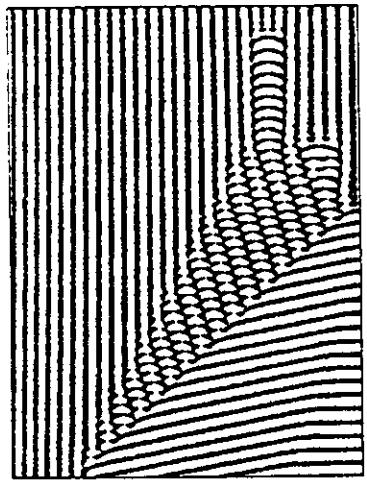

FIG. 4. Space-time map showing a Turing mode invading a Hopf background in a system of length 300 during 200 units of time. No-flux BC are applied. The mean velocity of the front is slower than one Turing wavelength for one temporal oscillation and hence the system evolves through intermediate localized oscillations. The initial condition is a stable front obtained for the same values of parameters as in Fig. 2 and $B=9$. The front is set unstable by suddenly decreasing B to 8.8 in order to go outside the pinning domain.

plest mode locking is one wavelength for one frequency but other ratios are possible as long as there is an integer number of wavelengths per period of oscillation or vice versa. In these situations, the front may progress faster or slower and, in order to satisfy the nonadiabatic constraint, the system then sometimes creates temporary localized subzones (Fig. 4) [30].

Two Turing-Hopf fronts can be used to build up stable localized structures corresponding to a droplet of a Turing (Hopf) state embedded into a Hopf (Turing) domain [Figs. 2(b) and 2(c)]. We observe that, if the Turing core contains several wavelengths, the stability region of such localized structures is the same as that of the front (Fig. 3) and can correspondingly be ascribed to pinning effects. Such localized structures are thus also stabilized by nonadiabatic effects. If the localized Turing domain contains few wavelengths, this stabilizing nonadiabatic effect can no longer be invoked alone. Stable localized Turing patterns with few wavelengths are nevertheless observed in the Brusselator model and the fewer wavelengths they contain, the largest their stability domain (Fig. 3). Their stability should then result from nonvariational effects present in the Brusselator as this model cannot be derived from any potential function. Nonvariational effects have been shown in other systems to stabilize localized structures if they provide a repulsive interaction between two fronts that otherwise attract each other [1,32,33]. They can thus account for the existence of localized droplets of one state embedded into the other state. This effect is strongest for the so-called "flip-flop" localized pattern having the smallest core [Fig. 2(d)] and therefore the widest stability domain. This could explain why the "flip-flop" is the only localized pattern that has been observed experimentally in the CIMA reaction for values of the concentrations near the CTHP [9]. Its two-dimensional extension, a Turing spot sitting in the core of a one-armed spiral, has also been obtained both in numerical simulations [29] and in the CIMA experiments [34]. Turing-Hopf localized structures have also been observed experimentally in one-dimensional arrays of resistively coupled nonlinear LC oscillators [10] and in binary-fluid convection [11].

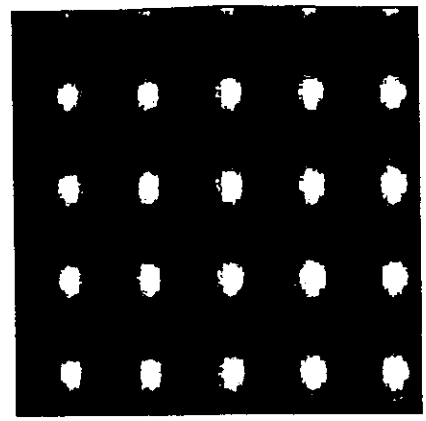

FIG. 5. Space-time map of the mixed mode with one wave number and one frequency for $A=0.8$, $D_v=10$, $\sigma/\sigma_c=0.9$, $B=1.68$, $L=64$ during 25 units of time. Periodic BC are applied.

Bistability between the Turing and Hopf modes near a CTHP had already long been predicted in the amplitude equation formalism. We have shown that in this bistability regime, localized structures of one state embedded into the other can be stabilized by a combination of nonadiabatic and nonvariational effects. In addition, if long-wavelength instabilities are considered, the Hopf mode could undergo a Benjamin-Feir instability and the Turing mode an Eckhaus instability [1]. These types of secondary instabilities have not been considered here.

B. Mixed mode and spatiotemporal chaos

Near the CTHP, the system may also exhibit a stable mixed mode corresponding to a spatial pattern with the Turing wave number oscillating in time with the Hopf frequency. This stable state has been obtained by numerical integration of the Brusselator model with periodic boundary conditions in both H-MM-T and T-MM-H cases. A space-time map of this dynamics (Fig. 5) shows the polygonal space-time structure characteristic of a mixed mode. This solution was previously obtained in numerical simulations of the Brusselator by Sangalli and Chang [35] in a H-MM-T scenario. Here we recover several of these scenarios in the $(A,\sigma/\sigma_c)$ parameter space but we also find the complementary T-MM-H scenario. This invalidates the conclusions of Rovinsky and Menzinger [36] stating that the MM is always unstable in the Brusselator.

The amplitude equations we have considered to predict the MM do not contain any spatial dependence of the amplitudes on the large scales. If such a dependence is taken into account, phase stability criteria can be derived giving the conditions for which the global solutions and the MM in particular [23] can become unstable towards secondary long-wavelength instabilities. In our simulations of the Brussela-

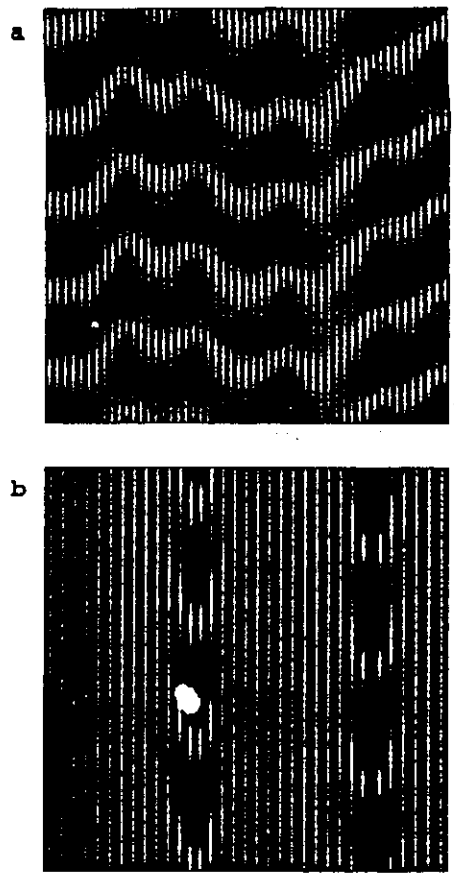

FIG. 6. Dynamics of the mixed mode in a large system. The dynamics is shown during 40 units of time with periodic BC. (a) Phase chaos. All parameters are the same as in Fig. 5 except $L=512$. (b) Localized MM embedded in the Turing regime obtained for $A=0.8$, $D_y=10$, $\sigma/\sigma_c=0.75$, $B=1.780$, $L=512$.

tor model, such a phase instability has been obtained. Using the size L of the system as a bifurcation parameter, the mixed mode of Fig 5. becomes phase unstable when L is increased and the system enters a regime of spatiotemporal chaos [Fig. 6(a)]. The fact that this chaos appears when using the length of the system as a control parameter suggests that we are here dealing with a long-wavelength instability and not with a homoclinic type of chaos. More complex spatiotemporal dynamics are obtained like the one displayed in Fig. 6(b): the stable MM appears as localized structures in a Turing pattern when the size of the system is increased. This mixed mode, generic of the CTHP, is characterized by one wave number k_c and one frequency ω_c. Other types of mixed modes can also be observed close to the CTHP as we will see next.

III. SUBHARMONIC INSTABILITY OF A TURING MODE

A mixed state different from the (k_c,ω_c) mixed mode discussed above (Fig. 5) has also been obtained in the Brusselator. This mixed state is characterized by one frequency and two wave numbers, the Turing one k_c and its subharmonic $k_c/2$. At each location, the system is oscillating in time and therefore the minima of the mixed state are shifted one wavelength each half period of oscillations. The corresponding space-time map of this dynamics (Fig. 7) concentrates all this information. We have drawn in Fig. 8 a schematic dispersion relation of the Brusselator model. Let us suppose that the primary bifurcation leads to the Turing state with wave number k_c. As we are close to the CTHP, the linear eigenvalue of the subharmonic mode with wave number $k_c/2$ may be complex with frequency $\omega(k_c/2)$ and its growth rate small. In the vicinity of such a critical situation [37], the variables of the system are expanded as

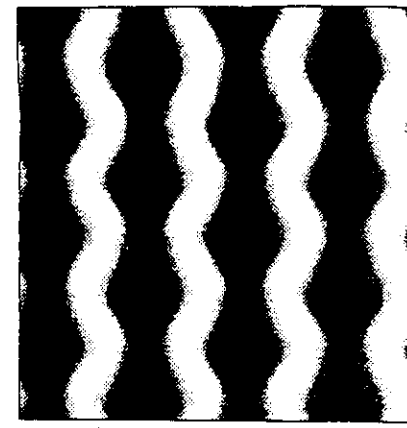

FIG. 7. Space-time map of the Y variable of the Brusselator shown in gray scale ranging from its minimum (white) to its maximum (black) value. The dynamics features a subharmonic Turing mode with two wave numbers and one frequency shown during 35 units of time. The parameters are $A=1.5$, $D_y=10$, $\sigma/\sigma_c=0.75$, $B=4.4$, $L=64$. Periodic BC are applied.

$$\mathbf{C}(x,t)=\mathbf{C}_0+Te^{ik_cx}\mathbf{w}_T+A_Le^{i[\omega(k_c/2)t+(k_c/2)x]}\mathbf{w}_L+A_Re^{i[\omega(k_c/2)t-(k_c/2)x]}\mathbf{w}_R+\text{c.c.}, \quad (5)$$

where $\mathbf{w}_L$ and $\mathbf{w}_R$ are the critical eigenvectors correspond-

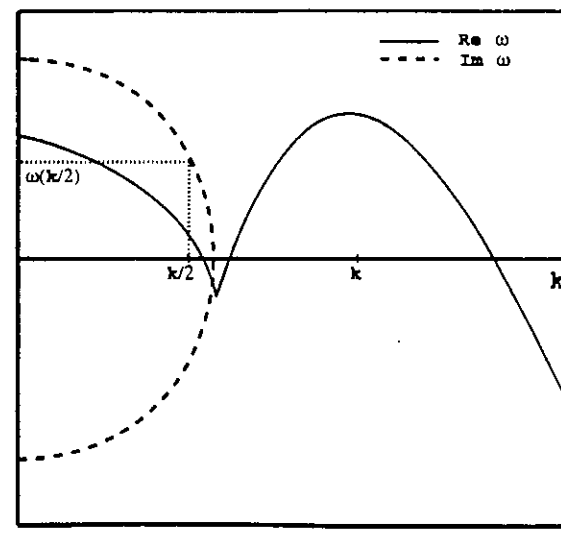

FIG. 8. Schematic dispersion relation explaining the resonance between the Turing mode $(k,0)$ and the subharmonic mode $[k/2,\omega(k/2)]$ leading to the existence of the sub$T$ mode of Fig. 7. The solid (dashed) line corresponds to the k dependence of the solid real (imaginary) part of the eigenvalues of the linear stability analysis.

ing to the left- and right-going waves of wave number $k_c/2$ and frequency $\omega(k_c/2)$. The amplitudes obey the following equations [38,39]:

$$\frac{\partial T}{\partial t}=\mu T-g|T|^2T-\lambda(|A_R|^2+|A_L|^2)T+\upsilon A_R^*A_L, \quad (6)$$

$$\frac{\partial A_R}{\partial t}=\mu' A_R-g'|A_R|^2A_R-h'|A_L|^2A_R-\lambda'|T|^2A_R+\upsilon' T^*A_L, \quad (7)$$

$$\frac{\partial A_L}{\partial t}=\mu' A_L-g'|A_L|^2A_L-h'|A_R|^2A_L-\lambda'|T|^2A_L+\upsilon' TA_R, \quad (8)$$

where μ', g, and λ are taken as real while the primed coefficients are complex ($\alpha'=\alpha_r'+i\alpha_i'$). All bifurcations are considered here to be supercritical with h_r' and λ_r' taken as positive. Among others, this system admits the following global solutions [39,40]: (1) a Turing mode: $T=\{\mu/g\}^{1/2}$, $A_R=A_L=0$; (2) a right traveling wave: $T=0$, $A_R=\{\mu'/g_r'\}^{1/2}e^{i\Omega_w t}$, $A_L=0$ or a left traveling wave: $T=0$, $A_R=0, A_L=\{\mu'/g_r'\}^{1/2}e^{i\Omega_w t}$ with the renormalization frequency $\Omega_w=-g_i'\mu'/g_r'$; and (3) a mixed mode solution $T=T_T$, $A_R=R_Te^{i(\Omega_T t+\phi_R)}$, $A_L=R_Te^{i(\Omega_T t+\phi_L)}$. By an appropriate choice of the origin of the coordinates, we can take T_T as real. The phases obey the equation

$$\frac{\partial(\phi_R-\phi_L)}{\partial t}=-2\upsilon_r'T_T\sin(\phi_R-\phi_L). \quad (9)$$

The $\phi_R-\phi_L=0$ (π) stationary solution is stable when $\upsilon_r'>0$ (<0). Then T_T, R_T, and Ω_T are the solutions of the following set of equations:

$$R_T^2=\frac{\mu'-\lambda_r'T_T^2+|\upsilon_r'|T_T}{g_r'+h_r'}, \quad (10)$$

$$0=gT_T^3-(\mu-2\lambda R_T^2)T_T\mp\upsilon R_T^2, \quad (11)$$

$$\Omega_T=\pm\upsilon_i'T_T-(g_i'+h_i')R_T^2-\lambda_i'T_T^2. \quad (12)$$

The upper (lower) sign in front of the υ's corresponds to the case where $\upsilon_r'>0$ (<0). The most prominent feature of Eqs. (6)–(8) is the presence of the resonant interaction term between the two modes $(k_c,0)$ and $[k_c/2,\omega(k_c/2)]$ proportional to υ and υ' which can induce a subharmonic destabilization of the Turing mode giving rise to a new mixed mode solution. A linear stability analysis of the solutions to (6)–(8) shows indeed that the Turing solution is the first to appear supercritically when $\mu'<\mu$ and $g>0$. This pure Turing mode becomes unstable towards the traveling wave if

$$\mu'>\lambda_r'\frac{\mu}{g} \quad (13)$$

and unstable towards the mixed mode solution when

$$\mu'>\lambda_r'\frac{\mu}{g}-|\upsilon_r'|\sqrt{\frac{\mu}{g}}. \quad (14)$$

As this mixed mode results from a subharmonic instability of the Turing pattern, let us coin it the subharmonic Turing mixed mode or in short sub$T$. A comparison of (13) and (14) shows that the first instability of the Turing mode will always be towards the sub$T$ rather than towards the traveling waves. This transition may be subcritical. The sub$T$ solution is the combination of a steady structure with wave number k_c and of a standing wave formed by the superposition of the left- and right-going waves ($A_R=A_L$) with wave number $k_c/2$ and frequency $\omega(k_c/2)$. The resulting spatiotemporal dynamics thus corresponds to a spatial pattern with two wave numbers oscillating in time with one frequency as observed in the Brusselator model (Fig. 7). The two wave numbers are here, respectively, the Turing wave number and its subharmonic. This mixed state is thus of a different origin than the one due to the interaction between a steady pattern and a wave as introduced in [7] where the two wave numbers are not necessarily linked. To find if the sub$T$ solution is stable towards perturbations of its amplitude, we insert $T=T_T+\delta_T$, $A_R=A_L=(R_T+\delta_R)e^{i\Omega_T t}$ into (6)–(8) and find the characteristic equation

$$\omega^2-a\omega+b=0, \quad (15)$$

with

$$a=-2gT_T^2\mp\upsilon\frac{R_T^2}{T_T}-2R_T^2(g_r'+h_r'), \quad (16)$$

$$b=2R_T^2\left\{\left[2gT_T^2\pm\upsilon\frac{R_T^2}{T_T}\right](g_r'+h_r')-(|\upsilon_r'|-2\lambda_r'T_T)(\pm\upsilon-2\lambda T_T)\right\}. \quad (17)$$

When the Turing mode (with $R_T=0$, $T_T=\sqrt{\mu/g}$) becomes unstable, a transition towards a stable sub$T$ mode occurs if $b>0$, i.e.,

$$2\mu(g_r'+h_r')-\left(\upsilon-2\lambda\sqrt{\frac{\mu}{g}}\right)\left(\upsilon_r'-2\lambda_r'\sqrt{\frac{\mu}{g}}\right)>0 \quad (18)$$

and if $a<0$. On the other hand, if $a>0$, the sub$T$ solution can undergo a Hopf instability of its amplitude that should give rise to chaotic behaviors. It is worthwhile to note that the sub$T$ mode can be obtained for values of parameters such that the standing waves of the system (7) and (8) with $T=0$ are unstable versus traveling waves ($h_r'>g_r'$). It is known that such a standing wave can be stabilized if an external time modulation with a frequency twice the frequency of the traveling waves is applied to the system [41,42]. Here the stabilization of the standing wave is self-induced by an intrinsic coupling with the steady mode which plays the role of an external forcing by restoring the left-right symmetry. The sub$T$ mode described here analytically has been observed in the Brusselator for $A=1.5$ when $\sigma/\sigma_c<1$. Looking at Fig. 9, we see that for the same A the

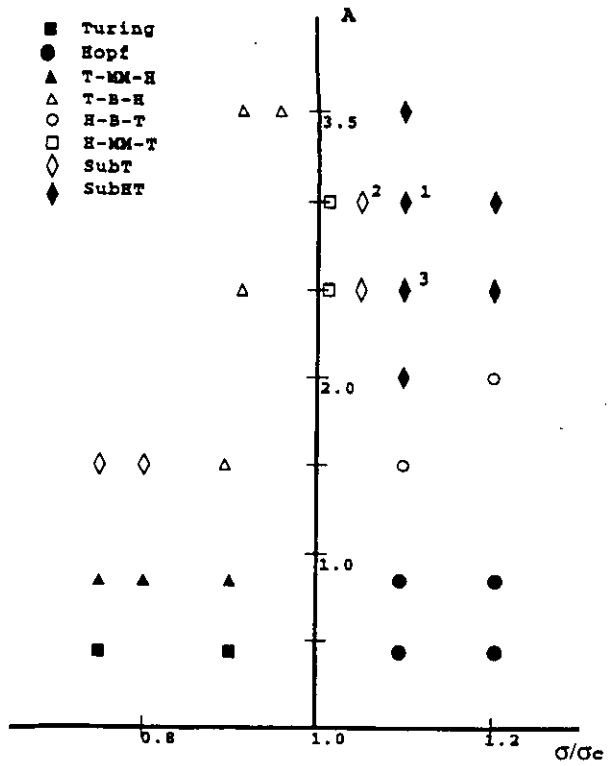

FIG. 9. Summary of the different spatiotemporal dynamics that can be observed in the Brusselator model near a codimension-two Turing-Hopf point in the parameter space $A-\sigma/\sigma_c$. The line $\sigma/\sigma_c=1$ is the codimension-two Turing-Hopf line. If $\sigma/\sigma_c<1$ (>1), the Turing (Hopf) bifurcation is the first to occur at criticality. The filled squares (circles) are points for which we have obtained only Turing (Hopf) states for all the values of B and the initial conditions we have scanned. The filled triangles represent points for which we obtain by increasing B successive transitions between a Turing mode—a mixed mode with one wave number and one frequency (see Fig. 5)—a Hopf mode. The reverse situation with the Hopf mode being the first to appear exists for the open squares. Bistability regimes with the corresponding localized structures (see Fig. 2) obtained after the Turing (Hopf) mode are observed at points with an open triangle (circle). Sub$T$ modes with two wave numbers and one frequency (see Figs. 7 and 14) are observed at points where an open diamond is pictured. Filled diamonds represent points where the subHT mode with two wave numbers and two frequencies (see Fig. 11) come to hand. Points 1–3 are the locations for which numerical bifurcation schemes are discussed in Sec. V.

T-B-H scheme exists near $\sigma/\sigma_c=1$, that is, near the CTHP line. Subharmonic instability of the Turing mode comes into play further away from this line. The sub$T$ mode is reminiscent of subharmonic cellular patterns observed experimentally in the flow of a viscous fluid inside a partially filled rotating horizontal cylinder [13]. In this experimental setup, successive transitions between steady patterns, the sub$T$ mode, and spatiotemporal chaos due to a phase instability of the sub$T$ mode [40] are observed when the control parameter is increased.

We have shown that near a CTHP, a Turing mode can give rise to subharmonic cellular patterns oscillating in time and generated by subharmonic instabilities. The same type of instability can destabilize the other generic solution of the system, i.e., the Hopf mode, as we will see in the next section.

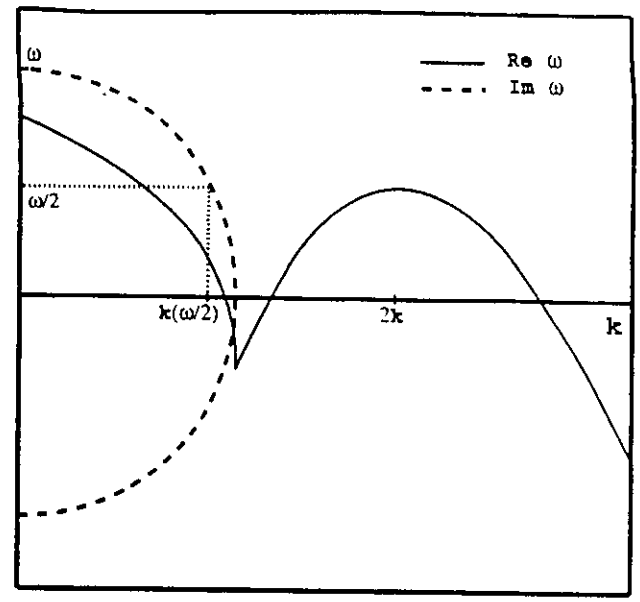

FIG. 10. Schematic dispersion relation explaining the resonance between the Hopf mode $(0,\omega)$ and the subharmonic mode $[k(\omega/2),\omega/2]$ leading to the existence of a sub$H$ mode with one wave number and two frequencies. If in addition $2k$ is of the order of the Turing wave number, the additional resonance with the mode $(2k,0)$ can lead to the existence of a subHT mode with two wave numbers and two frequencies. The solid (dashed) line corresponds to the k dependence of the real (imaginary) part of the eigenvalues of the linear stability analysis.

IV. SUBHARMONIC INSTABILITY OF A HOPF MODE

Another subharmonic instability could be observed if the base state is the Hopf mode with frequency ω_c generated by a primary bifurcation. The subharmonic mode $\omega_c/2$ has an eigenvalue of the linear stability analysis associated to a wave number $k(\omega_c/2)$ (Fig. 10). If a resonant interaction [43–45] occurs between the two modes $(0,\omega_c)$ and $[k(\omega_c/2),\omega_c/2]$, the variables of the system may be written as

$$\mathbf{C}(x,t)=\mathbf{C}_0+He^{i\omega_c t}\mathbf{w}_H+A_L e^{i[(\omega_c/2)t+k(\omega_c/2)x]}\mathbf{w}_L + A_R e^{i[(\omega_c/2)t-k(\omega_c/2)x]}\mathbf{w}_R+\text{c.c.}, \tag{19}$$

where the amplitudes obey the following equations:

$$\frac{\partial H}{\partial t}=\mu^H H-\beta|H|^2H-\gamma(|A_R|^2+|A_L|^2)H+\upsilon A_L A_R, \tag{20}$$

$$\frac{\partial A_R}{\partial t}=\mu'' A_R-\beta'|A_R|^2A_R-\gamma'|A_L|^2A_R-\delta'|H|^2A_R + \upsilon' HA_L^*, \tag{21}$$

$$\frac{\partial A_L}{\partial t} = \mu'' A_L - \beta' |A_L|^2 A_L - \gamma' |A_R|^2 A_L - \delta' |H|^2 A_L + v' H A_R^* . \quad (22)$$

All coefficients are complex ($\alpha = \alpha_r + i\alpha_i$). When $\mu_r'' < \mu_r^H$ a pure Hopf mode is the first to appear with $H = \sqrt{\mu_r^H/\beta_r} e^{i\Omega t}$; $A_R = A_L = 0$; $\Omega = -\beta_i \mu_r^H/\beta_r$. Here also the self-induced parametric terms proportional to v' favor the onset of modulated waves for which the three amplitudes are different from zero. Performing the linear stability analysis of the homogeneous oscillations with respect to perturbations $\delta R_R = \delta R_L = \delta R e^{i\psi}$ we find the instability condition:

$$\mu_r'' - \delta_r' \frac{\mu_r^H}{\beta_r} + \sqrt{\frac{\mu_r^H}{\beta_r}} [v_r' \cos 2\psi + v_i' \sin 2\psi] > 0, \quad (23)$$

where the phase ψ is determined by

$$\delta_i' \frac{\mu_r^H}{\beta_r} - \mu_i'' = \sqrt{\frac{\mu_r^H}{\beta_r}} [v_i' \cos 2\psi + v_r' \sin 2\psi]. \quad (24)$$

When the Hopf mode is unstable, another mixed state with now $H \neq 0$; $A_L = R_H e^{i\phi_L}$; $A_R = R_H e^{i\phi_R}$ can appear where H, R_H, and $\Phi = \phi_L + \phi_R$ are found as solutions of the following system of equations:

$$0 = \mu_r'' - [\beta_r' + \gamma_r'] R_H^2 - \delta_r' H^2 + H[v_r' \cos\Phi + v_i' \sin\Phi], \quad (25)$$

$$0 = \mu_i'' - [\beta_i' + \gamma_i'] R_H^2 - \delta_i' H^2 + H[v_i' \cos\Phi - v_r' \sin\Phi], \quad (26)$$

$$0 = \mu_r^H H - \beta_r H^3 - 2\gamma_r R_H^2 H + R_H^2 [v_r \cos\Phi - v_i \sin\Phi], \quad (27)$$

$$0 = -\beta_i H^3 - 2\gamma_i R_H^2 H + R_H^2 [v_r \sin\Phi + v_i \cos\Phi]. \quad (28)$$

As this other mixed mode results from a subharmonic instability of the homogeneous Hopf limit cycle, let us coin it the subharmonic Hopf mixed mode or in short sub$H$. This sub H mode is the combination of a homogeneous temporal oscillation with frequency ω_c and of a standing wave with frequency $\omega_c/2$ and wave number $k(\omega_c/2)$. The resulting dynamics is then a pattern with one wave number oscillating with two frequencies. This sub$H$ is different from the modulated standing waves occurring when homogeneneous and finite wave number Hopf instabilities interact [46]. We have not observed the sub$H$ dynamics in the Brusselator model although it should be generic as it is independent of the proximity of the CTHP contrary to the sub$T$ mode. Near the CTHP, we nevertheless observe a transition from a Hopf mode towards a mixed state with two wave numbers and two frequencies. We suggest that near the CTHP, a sub$H$ mode characterized by the wave number $k(\omega_c/2)$ could resonate with the Turing mode of wave number k_c if $2k \sim k_c$ (Fig. 10). In that case, the variables of the system would be given by

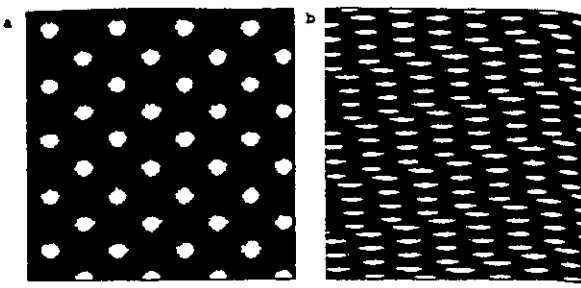

FIG. 11. Space-time maps of (a) the subHT mode with two frequencies and two wave numbers in a box of length $L = 80$ with periodic BC displayed during 25 units of time. The parameters are $A = 3$, $D_v = 10$, $\sigma/\sigma_c = 1.1$, $B = 10.445$. (b) Traveling subHT mode obtained for the same conditions as in (a) but with another random initial condition. The dynamics is shown during 100 units of time.

$$C(x,t) = C_0 + H e^{i\omega_c t} W_H + A_L e^{i[k(\omega_c/2)x + (\omega_c/2)t]} W_L + A_R e^{-i[k(\omega_c/2)x - (\omega_c/2)t]} W_R + T e^{2ikx} W_T + \text{c.c.}, \quad (29)$$

where the amplitudes obey a set of four coupled amplitude equations. We have not analyzed this set of equations but it seems reasonable to expect conditions for which a transition between a Hopf mode and a mixed state with two wave numbers and two frequencies is possible. As this spatiotemporal dynamics results from the resonance near the CTHP between a sub$H$ mode and a Turing mode, let us coin it the subHT mode. This subHT mode has been obtained in the Brusselator domain, for example, when $(A, \sigma/\sigma_c) = (3, 1.1)$. Starting from a homogeneous limit cycle at $B = 10.1$ in a system of length 64, a cellular pattern with two wavelengths appears with increasing amplitude when B is increased above 10.2. At each location of the system, the variables oscillate in time with two frequencies. After one period of oscillation, each maximum of the spatial pattern has become a minimum and vice versa. The initial structure is recovered after two periods as can be seen on the related space-time plot shown in Fig. 11(a). The same dynamics has been obtained in a reaction-diffusion model of a semiconductor device [47]. In the Brusselator, the subHT may also coexist with a traveling subHT mode [Fig. 11(b)].

Several mixed modes are stable near the CTHP in the Brusselator model: the simple MM, the sub$T$ mode, and the subHT. The transitions between those dynamics of the system can sometimes become very complex as we will see next.

V. ADDITIONAL SPATIOTEMPORAL DYNAMICS

To summarize the dynamics described up to now, let us look at Fig. 9, which displays the different bifurcation scenarios obtained numerically in the Brusselator model in the parameter space $(A, \sigma/\sigma_c)$. When $\sigma/\sigma_c < 1$, the Turing instability is the first one to be observed. For large values of

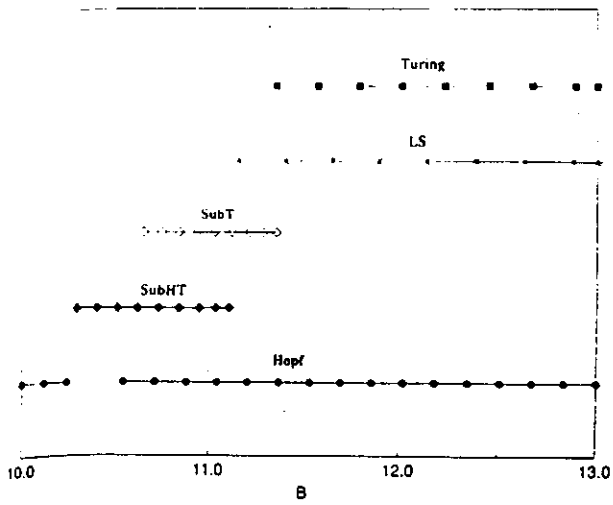

FIG. 12. Numerical bifurcation diagram obtained for the values of parameters of Fig. 11 (point 1 in Fig. 9). LS denotes localized structures (see Fig. 2). All other signs are as in Fig. 9.

A, the T-B-H scenario is at hand with its related dynamics such as Turing-Hopf fronts and localized structures. For small A's, the T-MM-H bifurcation scheme is obtained. This MM may give rise to phase chaos or localized structures in larger systems. The sub$T$ mode exists for intermediate A's but smaller σ/σ_c where the typical dynamics with two wave numbers and one frequency is observed. Eventually, for smaller σ/σ_c, the pure Turing mode is the only stable one we get.

For $\sigma/\sigma_c > 1$, the Hopf instability is the first one to be observed. For small A's, the pure Hopf mode is the only one existing. For intermediate A's, we get the H-B-T scenario and the related localized structures. For higher A's, the H-MM-T scheme is obtained near the $\sigma/\sigma_c = 1$ line while the H-subHT transition comes out for higher σ/σ_c. The situation on this side of the degeneracy line can nevertheless become quite complex as several bifurcation scenarios can mix at the same point $(A, \sigma/\sigma_c)$ when B is increased. To illustrate this, let us consider in detail three dynamical scenarios.

For $(A, \sigma/\sigma_c) = (3, 1.1)$ (point 1 in Fig. 9), the numerical bifurcation scenario obtained when B is increased is the following (Fig. 12): starting from a homogeneneous Hopf mode, a subharmonic instability towards the subHT mode of Fig. 11(a) occurs. This is the scenario explained in Sec. IV and which comes into play near criticality for several points in the $(A, \sigma/\sigma_c)$ plane. In addition this subHT mode coexists with a traveling subHT mode [Fig. 11(b)]. Above a certain value of B, the subHT mode enters a transient chaotic dynamics which eventually settles down on localized structures. These localized structures are bistable with the pure Turing and Hopf modes for higher B. In the intermediate region, a sub$T$ mode is also obtained. Its existence could be understood in terms of a T-sub$T$ transition when B is decreased. Unexpectedly, the T-sub$T$ transition can thus also be observed for $\sigma/\sigma_c > 1$ where the Hopf instability is the first to occur above criticality. We thus see that in a range of values of the control parameter B, there is coexistence of various types of spatiotemporal dynamics mixing several of the bifurcation schemes we have presented.

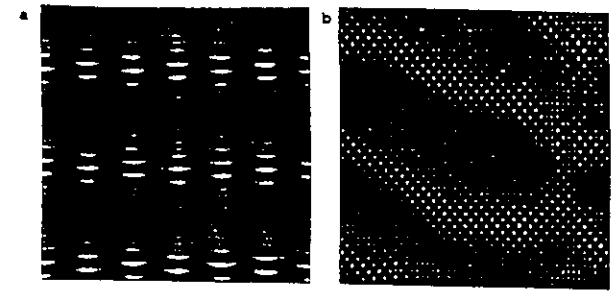

FIG. 13. Space-time map showing (a) the periodic incursion of a subHT mode into a pure Hopf mode in a system of size $L = 64$ for $A = 3$, $D_y = 10$, $\sigma/\sigma_c = 1.05$, $B = 10.3$ with periodic BC (point 2 in Fig. 9) during 25 units of time. (b) The same dynamics becomes unstable in a larger system of size $L = 512$.

In our second example, let us detail the bifurcation scheme at $(A, \sigma/\sigma_c) = (3, 1.05)$ (point 2 in Fig. 9). Near the threshold of instability $B = B_c^H$, the Hopf mode prevails. When B is increased, this Hopf mode becomes unstable: its amplitude begins to oscillate periodically and a subHT mode appears transiently in time [Fig. 13(a)]. Such a periodic incursion in time of the subHT mode can be explained in terms of a limit cycle instability of the four coupled amplitude equations that would admit the subHT mode as solution. The period of appearance of the subHT mode decreases when B is increased. This dynamics is unstable with respect to the phase when the size of the system is sufficiently large [Fig. 13(b)]. When $B = 10.4$, the system then evolves towards a stable Turing mode. This Turing mode further bifurcates towards a sub$T$ mode when B is further increased. This sub$T$ mode [Fig. 14(a)] here also coexists with a drifting sub$T$ mode [Fig. 14(b)]. Such a drifting mixed state was already seen by Sangalli and Chang [35] but in a Brusselator with differential convection. In our case, the dynamics is obtained without convection, which shows that the drifting sub$T$ mode is a solution totally intrinsic to the reaction-diffusion system near a CTHP [39]. It corresponds then to a mixed mode solution of the set of equations (6)–(8) for which

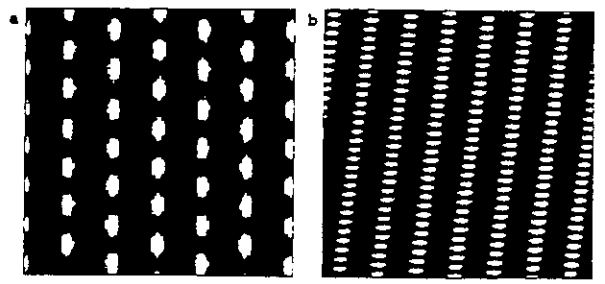

FIG. 14. Space-time maps of (a) a sub$T$ mode with two wave numbers and one frequency obtained for $A = 3$, $D_y = 10$, $\sigma/\sigma_c = 1.05$, $B = 10.45$, $L = 64$, periodic BC and shown during 25 units of time running upwards. Remark that $\sigma/\sigma_c > 1$. Hence the Hopf mode is the first to appear above the critical value of B. This sub$T$ mode exists only for higher values of B. (b) In a system of size $L = 80$ with periodic BC, an asymmetric subharmonic-Turing mixed mode is obtained for the same values of parameters as in (a). The dynamics is shown during 100 units of time.

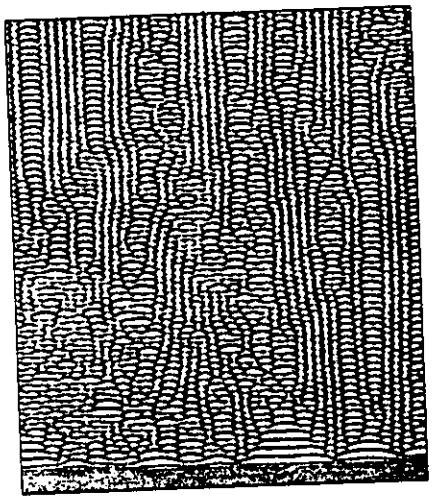

FIG. 15. Space-time map of a complex spatiotemporal dynamics obtained by starting from a random initial condition when $A=2.5$, $D_x=4.49$, $D_y=8.91$, $\sigma/\sigma_c=1.1$, $B=8$ (point 3 in Fig. 10) and no-flux BC are applied. $L=512$ and 300 units of time are shown. The same dynamics results when B is increased starting from a subHT mode stable for $B<7.8$.

$\sin(\phi_R-\phi_L)\neq 0$ and $R_R\neq R_L$. This conclusion is confirmed by numerical simulations of the Gray-Scott model near the CTHP by Rasmussen and Mazin [48] who also find bistability between the sub$T$ and the drifting sub$T$ mode. The overall bifurcation scheme for point 2 in Fig. 9 thus consists in the following succession of states: pure Hopf mode–heteroclinic appearance of the subHT mode–pure Turing mode–sub$T$ state coexisting with a traveling sub$T$ mode.

Our last example concerns the point $(A,\sigma/\sigma_c)=(2.5,1.1)$ (point 3 in Fig. 9). In this case, a change of the control parameter scans successive transitions [30] from a Hopf mode towards a subHT mode followed by spatiotemporal chaos (Fig. 15) and eventually localized structures characteristic of a bistability regime. The same behavior appears in the Gray-Scott model. In that case, the spatiotemporal chaos could be controlled to yield a stable Turing pattern [49].

The classification of the spatiotemporal dynamics near a CTHP in four scenarios: bistability, MM, sub$T$ or subHT thus allows description of most of the dynamics featured by a reaction-diffusion model.

VI. SUMMARY AND CONCLUSION

In this article, different bifurcation scenarios existing near a CTHP have been studied in the framework of amplitude equation formalism and used to understand and classify the numerical simulations of a reaction-diffusion model for values of parameters close to a CTHP. Two major families of spatiotemporal dynamics have been presented: those due to the interplay between the pure Turing and Hopf modes and those related to subharmonic instabilities of these modes.

When a Turing mode $T(k_c,0)$ interacts with a Hopf mode $H(0,\omega_c)$ near a CTHP, two types of behaviors can be obtained in addition to the existence of the pure modes.

(1) The Turing-Hopf bistability: in that case, the existence of nonadiabatic effects accounts for behaviors such as the stability of a simple Turing-Hopf front and of localized structures or a stepwise progression of this front depending on the values of parameters. Nonvariational effects contribute also to the existence of localized structures in the bistability domain of the two pure solutions. The existence of such a bistability domain and of the related localized structures has been obtained in the Brusselator model. Such localized structures have now been observed in several experimental systems [9–11].

(2) The Turing-Hopf mixed mode: spatial pattern characterized by one wave number and oscillating in time with one frequency. This mixed mode is generically observed in our reaction-diffusion model where it may also become phase unstable in large systems giving rise to spatiotemporal chaos.

The second major behaviors existing close to a CTHP appear when the pure modes are subjected to subharmonic instabilities. The resulting dynamics follow.

(1) The subharmonic Turing mixed mode, i.e., a cellular structure with two wave numbers oscillating in time with one frequency. This sub$T$ mixed mode has been observed in the Brusselator model where it may nevertheless appear as part of a much more complex overall bifurcation scheme. The transition bwtween a Turing state and a sub$T$ mode has also been seen experimentally in a hydrodynamical system where the subharmonic oscillating spatial pattern becomes phase unstable for higher values of the control parameter entering then a spatiotemporally chaotic regime [13].

(2) The subharmonic Hopf-Turing mixed mode corresponding to a biperiodic oscillation in time of a biperiodic modulation in space. This subHT mode exists in the Brusselator where it is bistable with other dynamics. It has also been observed in a reaction-diffusion model of a semiconductor device [47].

In addition to these major bifurcation schemes, we have identified in the $(A,\sigma/\sigma_c)$ phase space of the Brusselator three bifurcation scenarios that mix up the above classification.

To conclude, we have shown here that the amplitude equation formalism is a good basis to predict the spatiotemporal dynamics that can be observed near a CTHP. The bifurcation schemes predicted are recovered in the numerical integration of a reaction-diffusion model. These simulations confirm the theoretical predictions but also show some peculiarities of the dynamics that cannot be explained by the amplitude equations. In addition, the fact that different bifurcation schemes sometimes mixup when the control parameter is increased in the Brusselator points out the usefulness of the simulation of a model in parallel with the use of amplitude equations. As some of the spatiotemporal regimes presented here have been observed in experimental systems, we hope that the additional scenarios we have described will be observed in some physico-chemical systems featuring a degeneracy point where two instabilities breaking, respectively, space and time symmetries interact.

ACKNOWLEDGMENTS

D.L. is supported by the CNPQ/Brazil. A.D., G.D., and P.B. acknowledge financial support from the FNRS (Belgium).

[1] M.C. Cross and P.C. Hohenberg, Rev. Mod. Phys. **65**, 851 (1993).
[2] H.L. Swinney and J.P. Gollub, *Hydrodynamic Instabilities and Transition to Turbulence* (Springer, Berlin, 1985).
[3] *Nonlinear Optical Structures, Patterns, Chaos*, edited by L. A. Lugiato, special issue of Chaos, Solitons Fractals **4** (8,9) (1994).
[4] Physica A **188**, 1 (1992), special issue on nonequilibrium chemical dynamics, edited by F. Baras and D. Walgraef.
[5] *Chemical Waves and Patterns*, edited by R. Kapral and K. Showalter (Kluwer, Dordrecht, 1995).
[6] I. Rehberg and G. Ahlers, Phys. Rev. Lett. **55**, 500 (1985).
[7] B.J.A. Zielinska, D. Mukamel, and V. Steinberg, Phys. Rev. A **33**, 1454 (1986), and references therein.
[8] W. Zimmermann, D. Armbruster, L. Kramer, and W. Kuang, Europhys. Lett. **6**, 505 (1988), and references therein.
[9] J.-J. Perraud, A. De Wit, E. Dulos, P. De Kepper, G. Dewel, and P. Borckmans, Phys. Rev. Lett. **71**, 1272 (1993).
[10] G. Heidemann, M. Bode, and H.-G. Purwins, Phys. Lett. A **177**, 225 (1993).
[11] P. Kolodner, Phys. Rev. E **48**, R665 (1993).
[12] P. De Kepper, J.-J. Perraud, B. Rudovics, and E. Dulos, Int. J. Bif. Chaos **4**, 1215 (1994).
[13] D.P. Vallette, W.S. Edwards, and J.P. Gollub, Phys. Rev. E **49**, R4783 (1994).
[14] V. Castets, E. Dulos, J. Boissonade, and P. De Kepper, Phys. Rev. Lett. **64**, 2953 (1990).
[15] A. Turing, Philos. Trans. R. Soc. London, Ser. B **237**, 37 (1952).
[16] I. Lengyel and I.R. Epstein, Proc. Natl. Acad. Sci. (U.S.A.) **89**, 3977 (1992).
[17] G. Nicolis and I. Prigogine, *Self-Organization in Nonequilibrium Systems* (Wiley, New York, 1977).
[18] P. Borckmans, G. Dewel, A. De Wit, and D. Walgraef, in *Chemical Waves and Patterns*, edited by R. Kapral and K. Showalter (Kluwer, Dordrecht, 1995), p. 323.
[19] J.P. Keener, Stud. Appl. Math. **55**, 187 (1976).
[20] G. Nicolis, T. Erneux, and M. Herschkowitz-Kaufman, Adv. Chem. Phys. **38**, 263 (1978).
[21] H. Kidachi, Prog. Theor. Phys. **63**, 1152 (1980).
[22] J. Guckenheimer and P. Holmes, *Nonlinear Oscillations, Dynamical Systems, and Bifurcations of Vector Fields* (Springer-Verlag, New York, 1983).
[23] A. De Wit, G. Dewel, and P. Borckmans, Phys. Rev. E **48**, R4191 (1993).
[24] J. Verdasca, A. De Wit, G. Dewel, and P. Borckmans, Phys. Lett. A **168**, 194 (1992).
[25] Y. Pomeau, Physica D **23**, 3 (1986).
[26] D. Bensimon, B.I. Shraiman, and V. Croquette, Phys. Rev. A **38**, 5461 (1988).
[27] B.A. Malomed, A.A. Nepomnyashchy, and M.I. Tribelskii, Phys. Rev. A **42**, 7244 (1990).
[28] O. Jensen, V.O. Pannbacker, G. Dewel, and P. Borckmans, Phys. Lett. A **179**, 91 (1993).
[29] O. Jensen, V.O. Pannbacker, E. Mosekilde, G. Dewel, and P. Borckmans, Phys. Rev. E **50**, 736 (1994).
[30] A. De Wit, Ph.D. thesis, Université Libre de Bruxelles, 1993.
[31] P. Bak, T. Bohr, and M.H. Jensen, Phys. Scr. **T9**, 50 (1985).
[32] S. Koga and Y. Kuramoto, Prog. Theor. Phys. **63**, 106 (1980).
[33] O. Thual and S. Fauve, J. Phys. (Paris) **49**, 182 (1988).
[34] G. Dewel, P. Borckmans, A. De Wit, B. Rudovics, J.-J. Perraud, E. Dulos, J. Boissonade, and P. De Kepper, Physica A **213**, 181 (1995).
[35] M. Sangalli and H.-C. Chang, Phys. Rev. E **49**, 5207 (1994).
[36] A. Rovinsky and M. Menzinger, Phys. Rev. A **46**, 6315 (1992).
[37] A. Hill and I. Stewart, Dynam. Stab. Syst. **6**, 149 (1991).
[38] M. Cheng and H.-C. Chang, Phys. Fluids A **4**, 505 (1992).
[39] K. Fujimura and Y. Renardy, Physica D **85**, 25 (1995).
[40] D. Lima, A. De Wit, G. Dewel, and P. Borckmans, Phys. Rev. E **53**, 1305 (1996).
[41] H. Riecke, J.D. Crawford, and E. Knobloch, Phys. Rev. Lett. **61**, 1942 (1988).
[42] P. Coullet, K. Emilsson, and D. Walgraef, Physica D **61**, 132 (1992).
[43] M. Cheng and H.-C. Chang, Phys. Fluids A **7**, 34 (1995).
[44] R.E. Kelly, J. Fluid Mech. **27**, 657 (1967).
[45] P.A. Monkewitz, J. Fluid Mech. **188**, 223 (1988).
[46] H. Levine and X. Zou, Phys. Rev. E **48**, 50 (1993).
[47] A. Wacker, S. Bose, and E. Schöll, Europhys. Lett. **31**, 257 (1995).
[48] K.E. Rasmussen and W. Mazin, M.Sc. thesis, The Technical University of Denmark, 1994.
[49] V. Petrov, S. Métens, P. Borckmans, G. Dewel, and K. Showalter, Phys. Rev. Lett. **75**, 2895 (1995).